

THESIS FOR THE DEGREE OF DOCTOR OF PHILOSOPHY
IN
THERMO AND FLUID DYNAMICS

Development of adjoint-based optimization methods for
ducted flows in vehicles

EYSTEINN HELGASON

Department of Applied Mechanics
Division of Fluid Dynamics
CHALMERS UNIVERSITY OF TECHNOLOGY
Göteborg, Sweden 2015

Development of adjoint-based optimization methods for ducted flows in vehicles
EYSTEINN HELGASON
ISBN 978-91-7597-150-6

© EYSTEINN HELGASON, 2015

Doktorsavhandlingar vid Chalmers tekniska högskola
Ny serie nr. 3831
ISSN 0346-718X
Department of Applied Mechanics
Division of Fluid Dynamics
Chalmers University of Technology
SE-412 96 Göteborg
Sweden
Telephone: +46 (0)31-772 1000

Chalmers Reproservice
Göteborg, Sweden 2015

Development of adjoint-based optimization methods for ducted flows in vehicles
Thesis for the degree of Doctor of Philosophy in Thermo and Fluid Dynamics
EYSTEINN HELGASON
Department of Applied Mechanics
Division of Fluid Dynamics
Chalmers University of Technology

ABSTRACT

Application of the adjoint method in computational fluid dynamics makes the calculation of gradients of objective functions with respect to many design parameters computationally affordable. The adjoint method can be applied in sensitivity analysis or gradient-based optimization, dominating other methods in terms of computational cost. Gradient-based optimization processes used in industrial settings generally depend on computationally expensive flow simulations to calculate the gradients. When applying traditional methods, e.g. methods based on finite difference, the number of simulations required for the gradient calculations increases drastically with an increasing number of design parameters. This typically leads to a limited number of design parameters being considered. The application of the adjoint method in computational fluid dynamics can make the gradient calculations virtually independent of the number of design parameters. This can result in a more flexible and robust optimization tool. This thesis includes optimization and sensitivity calculations where the adjoint method is applied. The aim of this work is to increase knowledge and experience in utilization of the adjoint method with a focus on ducted flows within the automotive industry. This was done by validating previously presented implementations, implementing new cost functions as well as introducing a new method for shape optimization. In the derivation of the adjoint Navier-Stokes equations applied in the current work, the continuous adjoint approach has been followed. The variation with respect to the turbulent viscosity and the density was assumed to be negligible, and simplifications suitable for ducted flows have been applied. The adjoint method was applied in gradient-based optimization processes with the aim of minimizing the total pressure drop through a pipe. The results of three different implementations of the adjoint method were compared on an industrially relevant geometry where the boundary conditions resemble conditions in a truck at cruising speed. A convection-diffusion equation has also been used to simulate species distribution. The relevant adjoint equations were implemented for incompressible and weakly compressible flows. Cost functions describing species distribution at the outlet and at the surface were introduced. Finally, the results of the gradient calculations using the adjoint implementation were compared to gradient calculations made using finite difference simulations for a simple two dimensional channel.

Keywords: computational fluid dynamics, ducted flow, optimization, sensitivities, continuous adjoint method, finite difference.

ACKNOWLEDGEMENTS

First I would like to express my gratitude to my supervisor Professor Siniša Kra-jnović for giving me the opportunity to work in this exciting field. His motivation and provision of a stimulating research atmosphere is greatly acknowledged.

I would like to thank Per Jonsson, Dennis Konstanzer, Mattias Chevalier, Magnus Berglund, Raymond Reinmann, Stephen Conway and Niklas Nordin from Scania for interesting and helpful discussions at the steering group meetings. I would also like to thank them for welcoming me during my two months stay in Södertälje.

Special thanks go to Carsten Othmer and Andreas Gitt-Gehrke from Volkswagen for inviting me to stay at VW Salzgitter while working on the cell sensitivities. I would also like thank them for the many helpful discussions and for always being available to answer my questions. I would also like to thank the many friends I made in Braunschweig for making my visits enjoyable, both at work and after-work. I had a really great time!

Many thanks go to my friends and colleagues at the division of Fluid Dynamics for the great working environment. I would like to thank my roommate Jan Östh for all the on project and off project discussions in Swedish. Egill, Haukur and Ragnar for all the coffee breaks, lunch breaks and lunch exercises during this time at Chalmers. Huadong for introducing me to Chinese food and generosity. Olle for giving me tips on how to improve my skiing and biking, two important fields to work on after long days at work. I would also like to thank Mikael Öhman for taking the time to create and share this Latex template, it has saved me a lot of work. The administrative support of Ulla Lindberg-Thieme and Monica Vargman is gratefully acknowledged. I would like to thank my family and my loving girlfriend Halla for their support and encouragement during this work.

Computational time at Swedish National Infrastructure for Computing (SNIC) at the Center for Scientific Computing at Chalmers (C3SE) is acknowledged. This research is funded by the Swedish Energy Agency (Sw. Energimyndigheten), the support of which is gratefully acknowledged. A grant received by Eysteinn Helgason from the Landsvirkjun Energy Research Fund is gratefully acknowledged.

LIST OF PUBLICATIONS

This thesis consists of an extended summary and the following appended papers:

- Paper I** E. Helgason and S. Krajnović. Aerodynamic Shape Optimization of a Pipe using the Adjoint Method. *ASME 2012 International Mechanical Engineering Congress & Exposition, 9-15 November (2012)*. DOI: 10.1115/IMECE2012-89396
- Paper II** E. Helgason and S. Krajnović. Optimization using Arbitrary Lagrangian-Eulerian formulation of the Navier-Stokes equations. *Journal of Fluids Engineering (Accepted)* (2015)
- Paper III** E. Helgason and S. Krajnović. “A comparison of adjoint-based optimizations for industrial pipe flow”. *Proceedings of the ASME 2014 4th Joint US-European Fluids Engineering Division Summer Meeting, FEDSM 2014, Collocated with the ASME 2014 12th International Conference on Nanochannels, Microchannels, and Minichannels*. Vol. 1C. Chicago, United States, Aug. 2014. DOI: 10.1115/FEDSM2014-21542
- Paper IV** E. Helgason and S. Krajnović. “Implementation of an adjoint-based optimization with scalar transport”. *Proceedings of the ASME 2014 International Mechanical Engineering Congress & Exposition*. IMECE2014. Montreal, Quebec, Canada, Nov. 2014
- Paper V** E. Helgason and S. Krajnović. “Adjoint method for transport of heat and species in internal automotive flows”. *Proceedings of the First Thermal and Fluids Engineering Summer Conference*. (Submitted). American Society of Thermal and Fluids Engineers. New York, United States, Aug. 2015

DIVISION OF WORK

- Paper I** Implementation of the cost function and coupling of the surface sensitivities to the mesh motion was implemented by Eysteinn Helgason. Simulations and analyses were performed by Eysteinn Helgason. The manuscript was written by Eysteinn Helgason with the help of Siniša Krajnović.
- Paper II** The original idea of using volume sensitivities came from Andreas Gitt-Gehrke at Volkswagen. Further development and implementation were done by Eysteinn Helgason. Simulations and analyses were performed by Eysteinn Helgason. The manuscript was written by Eysteinn Helgason with the help of Siniša Krajnović.
- Paper III** Implementation of the topological optimization was performed by Eysteinn Helgason. Implementations from paper I and II were used. Simulations and analyses were performed by Eysteinn Helgason. The manuscript was written by Eysteinn Helgason with the help of Siniša Krajnović.
- Paper IV** Implementation of the adjoint scalar equation was performed by Eysteinn Helgason. Simulations and analysis were performed by Eysteinn Helgason. The manuscript was written by Eysteinn Helgason with the help of Siniša Krajnović.
- Paper V** Implementation of the weakly compressible adjoint equations was performed by Eysteinn Helgason. Simulations and analyses were performed by Eysteinn Helgason. The manuscript was written by Eysteinn Helgason with the help of Siniša Krajnović.

OTHER PUBLICATIONS

Other publications related to the thesis by the author:

Paper A S. Krajnović, R. Lárusson, E. Helgason, and B. Basara. “PANS of Rudimentary Landing Gear”. *6th AIAA Theoretical Fluid Mechanics Conference*. Honolulu, United States, 27 - 30 June 2011

Paper B S. Krajnović, E. Helgason, and H. Hafsteinsson. “Aerodynamic Shape Optimization of High-Speed Trains”. *Proceedings of the First International Conference on Railway Technology: Research, Development and Maintenance, Civil-Comp Press, Paper 162*. Stirlingshire, UK, 2012

CONTENTS

Abstract	i
Acknowledgements	iii
List of publications	v
Contents	ix
I Extended Summary	1
1 Introduction	3
1.1 Background	3
1.2 The adjoint method	6
2 The continuous adjoint approach	9
2.1 Overview	9
2.2 The adjoint Navier-Stokes equations	11
2.2.1 Internal flow	13
2.2.2 Scalar transport	16
2.3 Application with weakly compressible flows	20
2.4 Cost functions	22
2.4.1 Total pressure drop	23
2.4.2 Species uniformity at the outlet	23
2.4.3 Species concentration at a surface selection	24
2.5 Sensitivity calculations	25
2.5.1 Surface sensitivities	25
2.5.2 Topological sensitivities	27
2.5.3 ALE sensitivities	28
3 Summary of papers	29
3.1 Paper I	29
3.2 Paper II	29
3.3 Paper III	29
3.4 Paper IV	30
3.5 Paper V	30
4 Unpublished results	31
4.1 Validation case for scalar transport	31
4.2 Species uniformity at the surface, incompressible solver	35

5	Concluding remarks	41
	References	43
A	Derivation of the adjoint Navier-Stokes equations	49
A.1	Integration by parts	49
A.2	Weakly compressible flow	51
II	Appended Papers I–V	55

Part I

Extended Summary

1 Introduction

This thesis focuses on the development and application of the adjoint method for ducted flows in the automotive industry. It consists of an extended abstract and five appended papers. The first chapter contains an introduction to the adjoint method and its application in the automotive industry. The adjoint equations are introduced in chapter two. The derivation of the adjoint Navier-Stokes equations are presented, including the different forms of the adjoint equations applied in the appended papers. This includes the cost functions applied and the gradient of the objective function with respect to the design parameters. Chapter three contains a brief summary of each of the appended papers. Chapter four includes results not already included in the papers. Concluding remarks are given in chapter five, which is followed by the appended papers.

1.1 Background

Computer aided engineering (CAE) includes most aspects of engineering analysis from simulations and validation to optimization. The application of CAE has become an important part of the design and development process of modern vehicles. It can decrease product development cost and speed up the development of new products by the use of computer simulations. The information obtained from the computer simulations can partially be used to replace expensive and time consuming physical testing. The use of CAE in the automotive industry can generally be divided into three stages [3]: Basic modeling and algorithm research, integration into the development process and the last stage, the active application of the method in the design and development phases. It is the first stage that drives the development of CAE methods. The current demand from consumers and governmental regulations, see Fig. 1.1, for more fuel efficient and environmentally friendly vehicles while at the same time desires for durability and performance push designers and engineers to find new solutions and improve current methods. The strategies applied to obtain these improvements depend on the respective area of CAE.

Computational fluid dynamics (CFD) is a part of computer aided engineering and at the same time a core element in the development process in the automotive industry. It is applied both externally, on parts of a car or a whole vehicle, and on internal components in the design process. In CFD, the time to set up simulations and prepare large geometries can be considerable. This is followed by creation of the computational domain and the flow simulation itself. The flow simulations performed for engineering applications are often computationally expensive, requiring high performance supercomputers. The external design of a vehicle is impacted by various other factors than aerodynamics. This includes regulations, traffic policies, fashion and saleability. These factors, which are summed up in the term “market” in [20], are often out of the range of engineers and limit the freedom of the designers. The internal components, such as ducts,

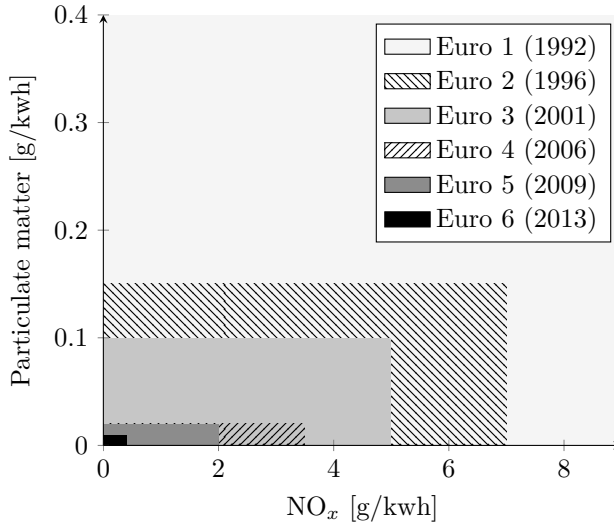


Figure 1.1: *European emission standards for trucks and buses, showing acceptable emission limits for new vehicles [21].*

are less likely to have to fulfill a fashion standard but are likely to be confined by packaging constraints. In the design process for a vehicle, the location of the major components is usually decided first, before the ducts that connect those components are designed. Getting all the components in place in the limited space of the underhood of today's vehicles can be a puzzle, see Fig. 1.2. The limited design space makes it a challenging task to design the ducts. This is where a robust and flexible optimization tool can be a valuable help in creating efficient ducts that are used to connect the different components in the vehicle. Optimization and flow control have been a subject of fluid dynamics for at least a century and, as noted in [11], usually consist of three main components. The first is the constraints which determine the type of flow being investigated. In the automotive industry, this can e.g. imply the incompressible Navier-Stokes equations. The second component is the objectives, that is what we want to control or minimize. Typical objectives for external aerodynamics are drag and lift force. For ducts, the aim can be to minimize losses through the pipe, maximize mixing or obtain uniform flow at the outlet. The third and last component is the controls or design parameters. This includes everything that can be used to meet the objective, e.g. the injection speed of a fluid injected into a stream or the parameters that are used to describe the geometry. Performing optimization using CFD is usually a computationally expensive task. In traditional optimization methods applied in the automotive industry, the number of flow simulations needed in the optimization process is highly dependent on the number of design parameters. With the high computational cost of each simulation and tight time constraints in modern industry, the solution can be to combine the design



Figure 1.2: *The underhood of modern vehicles can be tightly packed with components. Designing efficient ducts that connect the different components in this tightly packed compartment is not an easy task. Photo courtesy of Scania.*

parameters using only a few control points to describe the geometry. This applies e.g. to global optimization methods such as genetic and evolutionary algorithms, see e.g. [2].

Another type of optimization methods are so-called gradient based optimization methods. Gradient based optimization algorithms generally require a smooth and continuous objective function and converge to a local minimum. An example of a typical gradient based optimization process can be seen in Fig. 1.3. The optimization process begins by evaluating the objective function. This usually requires one flow simulation followed by an evaluation of the objective function. The next step is to calculate the gradients of the objective function with respect to the design parameters. This is normally the most time consuming part. The geometry is then modified using the information obtained from the gradient calculations, and the loop starts again. The loop continues until a certain criterion is fulfilled. An example of a simple gradient based algorithm is the steepest decent method. It is based on modifying a design parameter by moving in the direction of negative gradient of the objective function, i.e. a direction that decreases the objective function. This can be written as

$$\alpha_{\text{new}} = \alpha_{\text{old}} - \Delta \frac{\partial J(\alpha_{\text{old}})}{\partial \alpha_{\text{old}}}, \quad (1.1)$$

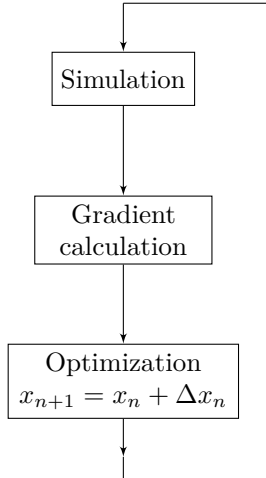


Figure 1.3: *Flow chart for a gradient based optimization method. The most time consuming part is usually the gradient calculations which limits the number of design variables used to describe the geometry.*

where J is the objective function, α is the design parameter and Δ is the step size. The last term can be approximated using a finite difference method such as the forward difference

$$\frac{\partial J}{\partial \alpha} \approx \lim_{h \rightarrow 0} \frac{J(\alpha + h) - J(\alpha)}{h}. \quad (1.2)$$

This requires one flow simulation to evaluate the objective function for the original geometry, $J(\alpha)$, and one simulation for each design parameter, $J(\alpha + h)$. This results in a total of $n + 1$ number of flow simulations for each loop in the gradient based optimization process, Fig. 1.3, where n is the number of design parameters. This approach therefore becomes computationally too expensive for most industrial applications when applied to a large number of design parameters. This part of the optimization process, i.e. the gradient calculations, is where application of the adjoint method is advantageous. It allows for the gradient calculations to be performed using only two solver calls, one for the primal flow solver and one for the adjoint solver. This makes the adjoint method an attractive choice for gradient calculations and sensitivity analysis when dealing with multiple design parameters in computationally expensive CFD simulations.

1.2 The adjoint method

The adjoint method has a history in optimal control theory dating back to the 1950s and has since been used in various different applications ranging from optimization in computer graphics [33] to pricing options in financial applications [1]. One

of the first appearances of the adjoint method in fluid dynamics is from 1973 when the continuous adjoint formulation of the Stokes equations was presented by Pironneau [45]. The application of the adjoint method gained popularity in the field of fluid dynamics following the publication of Jameson [23] in 1988, where he applied the adjoint Euler equations to transonic 2D airfoils and a decade later optimized a 3D wing using the adjoint Navier-Stokes equations [24]. Since then, multiple papers have been published on the application of the adjoint method in the field of aeronautics. These publications range from optimization of two dimensional airfoils for inviscid [27] and viscous flows [26] to optimization of wings [48] and complete aircraft configurations [8, 47, 46, 25]. The adjoint method has become an established method for sensitivity and gradient calculations in the aeronautics industry. At the same time, the automotive industry has been lagging behind. According to [40] there are two main reasons for this, the first one being that the car industry relies almost exclusively on commercial CFD software, opposed to in-house code, making the implementation of the adjoint equations practically impossible. Secondly, due to the high complexity of the parts being optimized in the automotive industry, the application of automatic tools for the creation of the computational meshes is favored over handmade meshes. The resulting computational grids can often lead to stability problems when performing adjoint simulations, which have proven to be more sensitive to mesh defects than general flow simulations. These problems can partially be overcome by introducing limiters to the adjoint equations.

The adjoint equations are generally derived by using either the continuous or the discrete approach, see Fig. 1.4. Both of the approaches start from the analytical form of the primal equations. In the continuous approach the primal equations are first linearized, the adjoint equations are then derived from the linearized primal equations and finally the adjoint equations are discretized. The discrete method starts with the discretization of the primal equations which are linearized and then finally transposed. Even though both implementations result in computationally inexpensive calculations of gradients for many design parameters, compared to direct methods, each of the two approaches has their advantages and disadvantages. One of the advantages of the discrete approach is that it gives the exact gradient of the discretized objective function and allows for the optimization process to converge fully. Automatic Differentiation (AD) tools can also be used in automation of the derivation of the source terms in the adjoint equations. Some of the advantages of the continuous adjoint equations are generally lower memory consumption and that the adjoint equations can be implemented in a straightforward manner in a C++ framework such as OpenFOAM® [38, 43]. Detailed discussions of the differences between the continuous and discrete implementation of the adjoint method can be found in [10, 36, 44, 9].

OpenFOAM (Open source Field Operation And Manipulation) is a C++ toolbox maintained by the OpenFOAM Foundation. It is mainly a computational fluid dynamics software package and includes a fair amount of pre- and post-processing utilities. Its syntax allows for the creation of custom solvers with relative ease. It was first released as open source in 2004 and has in recent years become more widely

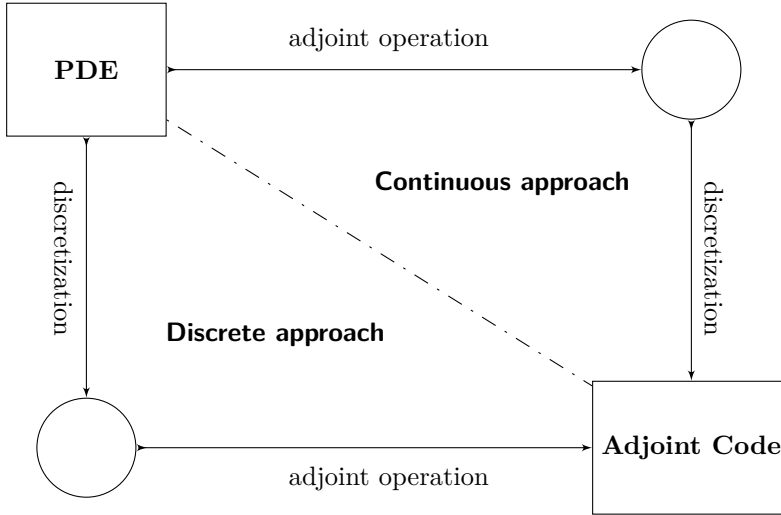


Figure 1.4: *The continuous vs the discrete adjoint approach. The continuous approach starts by deriving the adjoint equations in their analytical form and then discretizing the equations. The discrete adjoint approach on the other hand starts with the discretization of the equations and then transposing the equations in order to end at the adjoint code. The figure is a modified version of a figure presented in [9].*

used both in academia and in industry. The relatively simple implementation of custom solvers and its increasing popularity in industry are the main reasons behind choosing it as a CFD toolbox in this work. The first implementation of the continuous adjoint formulation of the Navier-Stokes equations in OpenFOAM was presented in 2008 [39]. Since then research groups at universities and from industry have published results from adjoint based sensitivity analysis and optimization using OpenFOAM. This includes optimization of exhaust systems [18, 19, 17], optimization of train head cars [22], buoyancy-driven flows with heat transfer [31], optimization of engine intake port [53] and mapping of surface sensitivities to morphing control points [42].

The next chapter describes the derivation of the adjoint equations applied in the appended papers.

2 The continuous adjoint approach

This chapter focuses on the derivation of the adjoint equations using the continuous approach and the implementations presented in the appended papers. It starts with a concise explanation of the derivation of the continuous adjoint equations. The steps outlined in this first section are pursued in the following sections. Section 2.2 outlines the derivation of the steady state, incompressible adjoint Navier-Stokes equations. It also includes simplifications made to the equations and boundary conditions for internal flow application. This is followed by the addition of a scalar transport equation. The adjoint equations for weakly compressible applications are shown in Section 2.3. The derivations are done for a generic cost function, with simplifications for internal flow. The cost functions applied in the appended papers are presented along with the relevant boundary conditions in Section 2.4. Finally, Section 2.5 describes how the gradient of the cost function with respect to the design changes applied in the appended papers is calculated from the primal and the adjoint field variables.

2.1 Overview

The adjoint method recently gained popularity in the field of computational fluid dynamics for its ability to drastically decrease the simulation time in gradient based optimization processes when dealing with a large number of design variables. The following is a brief explanation of the derivation of the continuous adjoint equations. For a more detailed explanation see e.g. [10, 9].

Given an objective function J , the total variation of J can be expressed as the sum of the variation with respect to the flow variables, \mathbf{w} , and the design variables, $\boldsymbol{\alpha}$,

$$\delta J = \underbrace{\frac{\partial J}{\partial \mathbf{w}} \delta \mathbf{w}}_{\text{flow}} + \underbrace{\frac{\partial J}{\partial \boldsymbol{\alpha}} \delta \boldsymbol{\alpha}}_{\text{design}}. \quad (2.1)$$

The flow equations in residual form can be written as

$$\mathbf{R}(\mathbf{w}, \boldsymbol{\alpha}) = \mathbf{0} \quad (2.2)$$

and, expressing the total variation of \mathbf{R} in the same way as the objective function, i.e. as the sum of the variation with respect to the flow variables, \mathbf{w} , and the design variables, $\boldsymbol{\alpha}$, yields

$$\delta \mathbf{R} = \frac{\partial \mathbf{R}}{\partial \mathbf{w}} \delta \mathbf{w} + \frac{\partial \mathbf{R}}{\partial \boldsymbol{\alpha}} \delta \boldsymbol{\alpha} = \mathbf{0}. \quad (2.3)$$

Now we can multiply Eq. (2.3) with an arbitrary Lagrange multiplier, $\boldsymbol{\lambda}$,

$$\boldsymbol{\lambda}^T \delta \mathbf{R} = \boldsymbol{\lambda}^T \frac{\partial \mathbf{R}}{\partial \mathbf{w}} \delta \mathbf{w} + \boldsymbol{\lambda}^T \frac{\partial \mathbf{R}}{\partial \boldsymbol{\alpha}} \delta \boldsymbol{\alpha} = 0. \quad (2.4)$$

By adding Eq. (2.4) to Eq. (2.1) the total variation of J can be expressed as

$$\delta L \equiv \delta J = \left[\frac{\partial J}{\partial \mathbf{w}} + \boldsymbol{\lambda}^T \frac{\partial \mathbf{R}}{\partial \mathbf{w}} \right] \delta \mathbf{w} + \left[\frac{\partial J}{\partial \boldsymbol{\alpha}} + \boldsymbol{\lambda}^T \frac{\partial \mathbf{R}}{\partial \boldsymbol{\alpha}} \right] \delta \boldsymbol{\alpha}. \quad (2.5)$$

It can be noted here that the variation of the Lagrangian, L , could also be defined by subtracting Eq. (2.4) from Eq. (2.1). We are now free to choose the value of the Lagrange multiplier so that the variation with respect to the flow variables vanishes, i.e.

$$\boldsymbol{\lambda}^T \frac{\partial \mathbf{R}}{\partial \mathbf{w}} \delta \mathbf{w} = - \frac{\partial J}{\partial \mathbf{w}} \delta \mathbf{w}. \quad (2.6)$$

The adjoint operator G^* to an operator G is defined as

$$\langle u, Gv \rangle = \langle G^*u, v \rangle \quad (2.7)$$

for all u and v , where the inner product is denoted by \langle, \rangle . Integrating by parts the left hand side of Eq. (2.6) results in a system of equations, the so called adjoint equations. Solving that system gives the values of the adjoint variables, the Lagrange multipliers. The total variation of the augmented objective function can then be written as

$$\delta L = \frac{\partial J}{\partial \boldsymbol{\alpha}} \delta \boldsymbol{\alpha} + \boldsymbol{\lambda}^T \frac{\partial \mathbf{R}}{\partial \boldsymbol{\alpha}} \delta \boldsymbol{\alpha} \quad (2.8)$$

where the variation is calculated using the variation of the objective function and an inner product between variation of the flow equations with respect to the design variable $\boldsymbol{\alpha}$ and the Lagrange multipliers, the solution to the adjoint equations.

One of the properties of the adjoint equations is that the propagation of information is reversed, compared to the primal equations. In the case of unsteady simulations the direction of the time integration changes, which has the effect that fully unsteady adjoint based design procedures are usually very memory demanding. In unsteady adjoint simulations, the primal flow field is calculated from the beginning to the end, as usual, and the adjoint flow is then solved backwards in time. The primal flow field needs to be retrieved at each point in time, either by storing all the primal flow time steps or by recalculating the primal flow field from a solution at a previous time step. The memory and computational requirements needed to store every time step make this very demanding for industrial applications. To limit the memory requirements, so called check pointing method can be used where a limited number of time steps, called check points, spread around the time line are saved. The primal simulations are then rerun and the intermediate time steps saved when the adjoint solver arrives at each of the check points [54, 35, 51]. An alternative approach compared in [34] is to use unsteady primal flow and steady adjoint solver for each time step or time averaged primal flow and steady adjoint solver to save computational time. In the current work, only steady simulations have been performed.

The next section describes the derivation of the adjoint equations when applying the steady state, incompressible Navier-Stokes equations as constraints.

2.2 The adjoint Navier-Stokes equations

The Navier-Stokes equations for an incompressible, single-phase, steady state flow consist of three momentum equations and a continuity equation,

$$\begin{aligned} (R_1, R_2, R_3)^T &= \rho u_j \frac{\partial u_i}{\partial x_j} + \frac{\partial p}{\partial x_i} - \frac{\partial}{\partial x_j} \left(\mu \left(\frac{\partial u_i}{\partial x_j} + \frac{\partial u_j}{\partial x_i} \right) \right), \\ R_4 &= -\frac{\partial u_i}{\partial x_i}, \end{aligned} \quad (2.9)$$

presented here in residual form where $u_{i=x,y,z}$ is the primal flow velocity vector, p is the primal pressure and ρ is the density. The viscosity term, μ , denotes the effective viscosity, i.e. the sum of the molecular and turbulent viscosity modeled by the eddy viscosity turbulence models. Einstein summation notation has been used, where repeated indices imply summation, and the comma in the indicial notation indicates a partial derivative with respect to each coordinate x_i , e.g. $\nabla \mathbf{u} = \frac{\partial u_j}{\partial x_i} = \partial_i u_j = u_{j,i}$.

Now we can set up an augmented cost function with the Navier-Stokes equations as the constraints:

$$L = J + \int_{\Omega} \boldsymbol{\lambda}^T \mathbf{R} \, d\Omega, \quad (2.10)$$

where J is the objective function we want to minimize and $\boldsymbol{\lambda}$ is a vector of the adjoint variables, $\boldsymbol{\lambda} = (\hat{u}_i, \hat{p})$, where \hat{u}_i is the adjoint velocity and \hat{p} is the adjoint pressure.

The total variation of L is:

$$\delta L = \underbrace{\delta_{\mathbf{w}} L}_{\text{flow}} + \underbrace{\delta_{\boldsymbol{\alpha}} L}_{\text{design}}. \quad (2.11)$$

The total variation of the Navier-Stokes equations is now split up into contributions from the flow field, \mathbf{w} , and the design variables, $\boldsymbol{\alpha}$:

$$\delta \mathbf{R} = \underbrace{\delta_{\mathbf{w}} \mathbf{R}}_{\text{flow}} + \underbrace{\delta_{\boldsymbol{\alpha}} \mathbf{R}}_{\text{design}}. \quad (2.12)$$

We focus now on the variation with respect to the flow field, which is the part where the adjoint equation system is solved. Setting the variation of the augmented cost function with respect to the flow variables, \mathbf{w} , to zero, as shown in Eq. (2.6), results in

$$\delta_{\mathbf{w}} L = \delta_{\mathbf{w}} J + \int_{\Omega} \boldsymbol{\lambda}^T \delta_{\mathbf{w}} \mathbf{R} \, d\Omega = 0. \quad (2.13)$$

The variation with respect to the flow field can further be split up into variation with respect to the primal flow field, \mathbf{u} , and the primal pressure, p ,

$$\delta_{\mathbf{w}} \mathbf{R} = \delta_{\mathbf{u}} \mathbf{R} + \delta_p \mathbf{R}. \quad (2.14)$$

The variation with respect to the flow field can now be written as:

$$\delta_{\mathbf{w}}L = \delta_{\mathbf{u}}J + \delta_p J + \int_{\Omega} (\hat{u}_i, \hat{p}) \delta_{\mathbf{u}} \mathbf{R} \, d\Omega + \int_{\Omega} (\hat{u}_i, \hat{p}) \delta_p \mathbf{R} \, d\Omega. \quad (2.15)$$

Writing out the variation with respect to the primal velocity flow field, $\delta_{\mathbf{u}} \mathbf{R}$, gives

$$\begin{aligned} \delta_{\mathbf{v}}(R_1, R_2, R_3)^T &= \rho \delta u_j u_{i,j} + \rho u_j \delta u_{i,j} - (\mu(\delta u_{i,j} + \delta u_{j,i}))_{,j}, \\ \delta_{\mathbf{v}} R_4 &= -\delta u_{i,i} \end{aligned} \quad (2.16)$$

and the variation with respect to the primal pressure, $\delta_p \mathbf{R}$, is

$$\begin{aligned} \delta_p(R_1, R_2, R_3)^T &= \delta p_{,i}, \\ \delta_p R_4 &= 0. \end{aligned} \quad (2.17)$$

The variation of the eddy viscosity, μ , has been neglected here and this assumption is exactly correct for laminar flow regions. This approximation is common in the derivation of the continuous adjoint Navier-Stokes equations, generally referred to as “frozen turbulence” [49, 24]. For recent developments in the field of continuous adjoint turbulence models and adjoint wall functions, see for example [55, 56]. There are varying views on the effect of this approximation from being almost negligible in engineering applications and leading to an error of the order of a few percent compared to the exact full adjoint based gradient [32] to in some cases errors up to 50% [37]. The memory requirements and run time are however undoubtedly considerably lower with the “frozen turbulence” assumption as no adjoint turbulence equations need to be solved. For a study of the effect of common approximations in the implementation of the adjoint method see e.g. [7].

Inserting the linearized constraints, Eq. (2.16) and Eq. (2.17), into Eq. (2.15) yields

$$\begin{aligned} 0 = \delta_{\mathbf{u}}J + \delta_p J + \int_{\Omega} (\hat{u}_i \rho \delta u_j u_{i,j} + \hat{u}_i \rho u_j \delta u_{i,j} - \hat{u}_i (\mu(\delta u_{i,j} + \delta u_{j,i}))_{,j} \\ + \hat{u}_i \delta p_{,i} - \hat{p} \delta u_{i,i}) \, d\Omega. \end{aligned} \quad (2.18)$$

Now we proceed to “move” the derivatives from the primal flow variables, δu_i and δp , to the adjoint variables, \hat{u}_i and \hat{p} , using integration by parts. The integration by parts is shown in full in Appendix A.1. After integrating by parts, the cost function is decomposed into contributions from the interior, Ω , and the boundary, Γ , i.e.

$$J = \int_{\Gamma} J_{\Gamma} \, d\Gamma + \int_{\Omega} J_{\Omega} \, d\Omega. \quad (2.19)$$

Equation (2.18) can now be replaced by

$$\begin{aligned}
0 &= \int_{\Omega} \left(\frac{\partial J_{\Omega}}{\partial u_i} - \rho \hat{u}_{j,i} u_j - \rho \hat{u}_{i,j} u_j - (\mu(\hat{u}_{i,j} + \hat{u}_{j,i}))_{,j} + \hat{p}_{,i} \right) \delta u_i \, d\Omega \\
&+ \int_{\Gamma} \left(\frac{\partial J_{\Gamma}}{\partial u_i} + \rho n_i \hat{u}_j u_j + \rho \hat{u}_i u_j n_j + \mu(\hat{u}_{i,j} + \hat{u}_{j,i}) n_j - \hat{p} n_i \right) \delta u_i \, d\Gamma \\
&- \int_{\Gamma} \mu \hat{u}_i (\delta u_{i,j} + \delta u_{j,i}) n_j \, d\Gamma \\
&+ \int_{\Omega} \left(\frac{\partial J_{\Omega}}{\partial p} - \hat{u}_{i,i} \right) \delta p \, d\Omega + \int_{\Gamma} \left(\frac{\partial J_{\Gamma}}{\partial p} + \hat{u}_i n_i \right) \delta p \, d\Gamma.
\end{aligned} \tag{2.20}$$

Combining the terms that depend on δu_i and δp and knowing that Eq. (2.20) is fulfilled for all variation of the primal flow field that satisfies the primal Navier-Stokes equations implies that each of the integrals must become zero independently of each other. From this condition on the integrals in Eq. (2.20), the adjoint Navier-Stokes equations can be derived as:

$$-\rho(\hat{u}_{j,i} + \hat{u}_{i,j})u_j = -\hat{p}_{,i} + (\mu(\hat{u}_{i,j} + \hat{u}_{j,i}))_{,j} - \frac{\partial J_{\Omega}}{\partial u_i}, \tag{2.21a}$$

$$\hat{u}_{i,i} = \frac{\partial J_{\Omega}}{\partial p}. \tag{2.21b}$$

With the following boundary conditions:

$$\begin{aligned}
0 &= \int_{\Gamma} \left(\frac{\partial J_{\Gamma}}{\partial u_i} + \rho n_i \hat{u}_j u_j + \rho \hat{u}_i u_j n_j + \mu(\hat{u}_{i,j} + \hat{u}_{j,i}) n_j - \hat{p} n_i \right) \delta u_i \, d\Gamma \\
&- \int_{\Gamma} \mu \hat{u}_i (\delta u_{i,j} + \delta u_{j,i}) n_j \, d\Gamma,
\end{aligned} \tag{2.22a}$$

$$0 = \int_{\Gamma} \left(\frac{\partial J_{\Gamma}}{\partial p} + \hat{u}_i n_i \right) \delta p \, d\Gamma \tag{2.22b}$$

The adjoint Navier-Stokes equations have some similarities with the primal Navier-Stokes equations. The main difference is however in the contribution from the objective function to the source terms and that the adjoint convection is upstream of the primal flow field, the first term on the left in the adjoint momentum equations.

2.2.1 Internal flow

The continuous adjoint equations and the boundary conditions presented in the previous section can be simplified for certain applications. This section focuses on simplifications that assume internal flow and follows the work done by Othmer in [39]. The adjoint Navier-Stokes equations in Eq. (2.21) accompanied by the boundary conditions in Eq. (2.22) can be simplified with respect to application in internal flow. Cost functions applied to internal flow simulations often include

only integrals over the surface, i.e. inlet, outlet and walls, and not the internal domain. Assuming that the cost function is zero inside the domain eliminates the last terms in Eqs. (2.21a) and (2.21b). This reduces the adjoint momentum and continuity equations to

$$-\rho(\hat{u}_{j,i} + \hat{u}_{i,j})u_j = -\hat{p}_{,i} + (\mu(\hat{u}_{i,j} + \hat{u}_{j,i}))_{,j}, \quad (2.23a)$$

$$\hat{u}_{i,i} = 0. \quad (2.23b)$$

This simplifies the implementation of new cost functions into the solver as the adjoint equations are now independent of the cost function. The cost function now only enters the boundary conditions of the adjoint velocity and pressure fields.

We follow the simplifications made by Othmer[39] and assume that part of the viscosity terms on the boundary can be neglected

$$\int_{\Gamma} \mu (\hat{u}_{j,i} n_j \delta u_i - \hat{u}_i \delta u_{j,i} n_j) \, d\Gamma \approx 0. \quad (2.24)$$

The boundary conditions that need to be fulfilled are now:

$$0 = \int_{\Gamma} \left(\frac{\partial J_{\Gamma}}{\partial u_i} + \rho n_i \hat{u}_j u_j + \rho \hat{u}_i u_j n_j + \mu \hat{u}_{i,j} n_j - \hat{p} n_i \right) \delta u_i \, d\Gamma \\ - \int_{\Gamma} \mu \hat{u}_i \delta u_{i,j} n_j \, d\Gamma, \quad (2.25a)$$

$$0 = \int_{\Gamma} \left(\frac{\partial J_{\Gamma}}{\partial p} + \hat{u}_i n_i \right) \delta p \, d\Gamma \quad (2.25b)$$

Some of the terms in the boundary conditions for the adjoint Navier-Stokes equations can be neglected by considering the three common boundaries in internal flow simulations, inlet, outlet and walls.

Inlet and walls: We usually have a prescribed value for the inlet velocity and a no-slip boundary condition for the walls, which results in $\delta u_i = 0$, and therefore the first integral in Eq. 2.25a is zero. For the second integral, by decomposing the δu_i term into contributions from the normal component to the surface, $n_i \delta u_i$, and the tangential component, $\delta \mathbf{u}_t = \delta u_i - n_i \delta u_i$, and then applying the continuity equation, $\delta u_{i,i} = 0$, assuming $\delta \mathbf{u}_t = \mathbf{0}$ at the inlet and walls, the remaining term from the continuity equation becomes

$$n_j (n_i \delta u_i)_{,j} = 0. \quad (2.26)$$

This decomposition of the continuity equation can be seen as

$$\nabla \cdot \delta \mathbf{u} = \underbrace{\frac{\partial \delta u_x}{\partial x}}_{\mathbf{n} \cdot \nabla (\delta \mathbf{u} \cdot \mathbf{n})} + \underbrace{\frac{\partial \delta u_y}{\partial y} + \frac{\partial \delta u_z}{\partial z}}_{\nabla_t \cdot \delta \mathbf{v}_t = 0} \quad (2.27)$$

in the case where the normal component to the surface, \mathbf{n} , is aligned along the x -axis. Using the same decomposition for the term in the second integral in

Eq. (2.25a), we get that

$$n_j \delta u_{i,j} = \underbrace{n_j (n_i \delta u_i)_{,j}}_{\rightarrow 0} + n_j (\delta u_t)_{,j} \quad (2.28)$$

From this we conclude that the tangential component of the adjoint velocity needs to be set to zero to fulfill the boundary conditions. No boundary condition is prescribed for the adjoint pressure, \hat{p} , and Neumann boundary conditions are applied, similar as for the primal pressure.

$$\hat{\mathbf{u}}_t = \mathbf{0}, \quad (2.29a)$$

$$n_i \hat{u}_i = -\frac{\partial J_\Gamma}{\partial p}, \quad (2.29b)$$

$$n_i \hat{p}_{,i} = 0. \quad (2.29c)$$

Outlet: For the outlet we have Neumann boundary conditions for velocity and the second integral of Eq. (2.25a) is zero. The pressure is set to zero at the outlet, so $\delta p = 0$ and the integral in Eq. (2.25b) is therefore zero. By splitting the first integral of Eq. (2.25a) into normal and tangential components, the boundary conditions for the adjoint pressure, \hat{p} , and the tangential component of the adjoint velocity can be determined as

$$\hat{p} = \frac{\partial J_\Gamma}{\partial (u_i n_i)} + \rho \hat{u}_j u_j + \rho \hat{u}_i n_i u_j n_j + \mu (n_i \hat{u}_i)_{,j} n_j, \quad (2.30a)$$

$$0 = \frac{\partial J_\Gamma}{\partial \mathbf{u}_t} + \rho \hat{\mathbf{u}}_t u_j n_j + \mu \hat{\mathbf{u}}_{t,j} n_j. \quad (2.30b)$$

The normal gradient of the normal component of the adjoint velocity, \hat{u}_i , is determined from the continuity equation using the same decomposition as shown in Eq. 2.27.

In the incompressible solvers in OpenFOAM[®], such as simpleFOAM, the momentum equations have been normalized with density and the pressure that is solved for is the normalized pressure. The adjoint equations presented here can easily be modified to fit these state equations. The state equations enter the adjoint equations through the constraints, \mathbf{R} , included in the augmented cost functional, L . By normalizing these terms with density, the resulting form of the adjoint momentum and continuity equations is

$$-\left(\frac{\partial \hat{u}_j}{\partial x_i} + \frac{\partial \hat{u}_i}{\partial x_j} \right) u_j = -\frac{\partial \bar{\hat{p}}}{\partial x_i} + \frac{\partial}{\partial x_j} \left(\nu \left(\frac{\partial \hat{u}_i}{\partial x_j} + \frac{\partial \hat{u}_j}{\partial x_i} \right) \right), \quad (2.31a)$$

$$\frac{\partial \hat{u}_i}{\partial x_i} = 0. \quad (2.31b)$$

There is no impact on the boundary conditions for the inlet and walls,

$$\hat{\mathbf{u}}_t = \mathbf{0}, \quad (2.32a)$$

$$n_i \hat{u}_i = -\frac{\partial J_\Gamma}{\partial p}, \quad (2.32b)$$

$$n_i \bar{\hat{p}}_{,i} = 0. \quad (2.32c)$$

For the outlet, all terms not including the cost function are normalized with density,

$$\bar{\hat{p}} = \frac{\partial J_\Gamma}{\partial(u_i n_i)} + \hat{u}_j u_j + \hat{u}_i n_i u_j n_j + \nu(n_i \hat{u}_i)_{,j} n_j, \quad (2.33a)$$

$$0 = \frac{\partial J_\Gamma}{\partial \mathbf{u}_t} + \hat{\mathbf{u}}_t u_j n_j + \nu \hat{\mathbf{u}}_{t,j} n_j. \quad (2.33b)$$

2.2.2 Scalar transport

This section describes the derivation of the adjoint scalar transport equation presented in [19]. The scalar transport equation can be used to describe the flow of particles, species or temperature due to diffusion and convection. The sensitivity of the scalar distribution with respect to modification of the design parameters can be calculated by applying the adjoint method. The aim can e.g. be to improve the scalar distribution at the surface or at the outlet of a duct. This is done by adding the scalar transport equation to the constraints in the augmented cost function. The steady state formulation of the scalar transport equation for incompressible flow, neglecting any source or sink terms, is

$$u_i \frac{\partial c}{\partial x_i} = \frac{\partial}{\partial x_i} \left(D \frac{\partial c}{\partial x_i} \right), \quad (2.34)$$

where u_i is the velocity obtained from the flow solver, c is the species or particle concentration and D is the diffusion coefficient. We write the scalar transport equation in residual form,

$$R_5 = u_j \frac{\partial c}{\partial x_j} - \frac{\partial}{\partial x_j} \left(D \frac{\partial c}{\partial x_j} \right). \quad (2.35)$$

The augmented cost function can be written as

$$L = J + \int_{\Omega} d\Omega \begin{bmatrix} \hat{u}_i \\ \hat{p} \\ \hat{c} \end{bmatrix} \cdot \begin{bmatrix} u_j \frac{\partial u_i}{\partial x_j} + \frac{\partial p}{\partial x_i} - \frac{\partial}{\partial x_j} \left(\nu \left(\frac{\partial u_i}{\partial x_j} + \frac{\partial u_j}{\partial x_i} \right) \right) \\ - \frac{\partial u_j}{\partial x_j} \\ u_j \frac{\partial c}{\partial x_j} - \frac{\partial}{\partial x_j} \left(D \frac{\partial c}{\partial x_j} \right) \end{bmatrix} \quad (2.36)$$

where \hat{u}_i , \hat{p} and \hat{c} are the adjoint velocity, adjoint pressure and adjoint scalar, respectively. Note that the momentum equation has been normalized with density,

as is done in the incompressible solvers in OpenFOAM. The total variation of the augmented cost function is now written as

$$\delta L = \delta_{\mathbf{u}}L + \delta_p L + \delta_c L + \delta_{\alpha}L. \quad (2.37)$$

As before, we set the total variation with respect to the flow variables to zero, i.e.

$$\delta_{\mathbf{u}}L + \delta_p L + \delta_c L = 0. \quad (2.38)$$

The variation of the momentum and the continuity equation, R_{1-4} , was presented in Sections 2.2 and 2.2.1 and the equations integrated by parts. We now focus on the additional scalar transport equation and calculate the variation with respect to the flow variables, u , p and c as

$$\delta_{\mathbf{u}}R_5 = \delta u_j c_{,j}, \quad (2.39a)$$

$$\delta_p R_5 = 0, \quad (2.39b)$$

$$\delta_c R_5 = u_j \delta c_{,j} - (D\delta c_{,j})_{,j}. \quad (2.39c)$$

Combining the terms in Eq. (2.39) and multiplying with the adjoint scalar yields

$$\int_{\Omega} (\hat{c} \delta u_j c_{,j} + \hat{c} u_j \delta c_{,j} - \hat{c} (D\delta c_{,j})_{,j}) \, d\Omega. \quad (2.40)$$

Each of the terms is now integrated by parts,

$$\begin{aligned} \int_{\Omega} \hat{c} \delta u_j c_{,j} &= \int_{\Gamma} n_j \hat{c} \delta u_j c \, d\Gamma - \int_{\Omega} (\hat{c} \delta u_j)_{,j} c \, d\Omega, \\ &= \int_{\Gamma} n_j \hat{c} \delta u_j c \, d\Gamma - \int_{\Omega} \hat{c}_{,j} \delta u_j c \, d\Omega - \int_{\Omega} \hat{c} \delta u_{j,j}^0 c \, d\Omega, \end{aligned} \quad (2.41a)$$

$$\begin{aligned} \int_{\Omega} \hat{c} u_j \delta c_{,j} &= \int_{\Gamma} \hat{c} u_j n_j \delta c \, d\Gamma - \int_{\Omega} (\hat{c} u_j)_{,j} \delta c \, d\Omega, \\ &= \int_{\Gamma} \hat{c} u_j n_j \delta c \, d\Gamma - \int_{\Omega} \hat{c}_{,j} u_j \delta c \, d\Omega - \int_{\Omega} \hat{c} u_{j,j}^0 \delta c \, d\Omega, \end{aligned} \quad (2.41b)$$

$$\begin{aligned} - \int_{\Omega} \hat{c} (D\delta c_{,j})_{,j} &= - \int_{\Gamma} n_j \hat{c} D\delta c_{,j} \, d\Gamma + \int_{\Omega} \hat{c}_{,j} D\delta c_{,j} \, d\Omega, \\ &= - \int_{\Gamma} n_j \hat{c} D\delta c_{,j} \, d\Gamma + \int_{\Gamma} n_j D\hat{c}_{,j} \delta c \, d\Gamma - \int_{\Omega} (D\hat{c}_{,j})_{,j} \delta c \, d\Omega. \end{aligned} \quad (2.41c)$$

The total variation with respect to the flow variables, Eq. (2.38), can now be written by adding the terms in Eq. (2.41) to Eq. (2.20),

$$\begin{aligned}
0 &= \int_{\Omega} \left(\frac{\partial J_{\Omega}}{\partial u_i} - \hat{u}_{j,i} u_j - \hat{u}_{i,j} u_j - (\nu(\hat{u}_{i,j} + \hat{u}_{j,i}))_{,j} + \hat{p}_{,i} \underbrace{-\hat{c}_{,i} c}_{(2.41a)} \right) \delta u_i \, d\Omega \\
&+ \int_{\Gamma} \left(\frac{\partial J_{\Gamma}}{\partial u_i} + n_i \hat{u}_j u_j + \hat{u}_i u_j n_j + \nu(\hat{u}_{i,j} + \hat{u}_{j,i}) n_j - \hat{p} n_i + \underbrace{\hat{c} c n_i}_{(2.41a)} \right) \delta u_i \, d\Gamma \\
&- \int_{\Gamma} \nu \hat{u}_i (\delta u_{i,j} + \delta u_{j,i}) n_j \, d\Gamma \\
&+ \int_{\Omega} \left(\frac{\partial J_{\Omega}}{\partial p} - \hat{u}_{i,i} \right) \delta p \, d\Omega + \int_{\Gamma} \left(\frac{\partial J_{\Gamma}}{\partial p} + \hat{u}_i n_i \right) \delta p \, d\Gamma \\
&+ \int_{\Omega} \left(\frac{\partial J_{\Omega}}{\partial c} - \hat{c}_{,j} u_j - (D\hat{c}_{,j})_{,j} \right) \delta c \, d\Omega \\
&+ \int_{\Gamma} \left(\frac{\partial J_{\Gamma}}{\partial c} + \hat{c} u_j n_j + Dn_j \hat{c}_{,j} \right) \delta c \, d\Gamma - \int_{\Gamma} \hat{c} Dn_j \delta c_{,j} \, d\Gamma
\end{aligned} \tag{2.42}$$

Knowing that Eq. (2.42) is fulfilled for all admissible variations of the flow variables yields the adjoint equations,

$$-(\hat{u}_{j,i} + \hat{u}_{i,j}) u_j = -\hat{p}_{,i} + (\nu(\hat{u}_{i,j} + \hat{u}_{j,i}))_{,j} + \hat{c}_{,i} c - \frac{\partial J_{\Omega}}{\partial u_i}, \tag{2.43a}$$

$$\hat{u}_{i,i} = \frac{\partial J_{\Omega}}{\partial p}, \tag{2.43b}$$

$$\hat{c}_{,j} u_j = -(D\hat{c}_{,j})_{,j} + \frac{\partial J_{\Omega}}{\partial c}. \tag{2.43c}$$

With the following boundary conditions,

$$\begin{aligned}
0 &= \int_{\Gamma} \left(\frac{\partial J_{\Gamma}}{\partial u_i} + n_i \hat{u}_j u_j + \hat{u}_i u_j n_j + \nu(\hat{u}_{i,j} + \hat{u}_{j,i}) n_j - \hat{p} n_i + \hat{c} c n_i \right) \delta u_i \, d\Gamma \\
&- \int_{\Gamma} \nu \hat{u}_i (\delta u_{i,j} + \delta u_{j,i}) n_j \, d\Gamma,
\end{aligned} \tag{2.44a}$$

$$0 = \int_{\Gamma} \left(\frac{\partial J_{\Gamma}}{\partial p} + \hat{u}_i n_i \right) \delta p \, d\Gamma, \tag{2.44b}$$

$$0 = \int_{\Gamma} \left(\frac{\partial J_{\Gamma}}{\partial c} + \hat{c} u_j n_j + Dn_j \hat{c}_{,j} \right) \delta c \, d\Gamma - \int_{\Gamma} \hat{c} Dn_j \delta c_{,j} \, d\Gamma. \tag{2.44c}$$

Following the arguments given in Section 2.2.1, the adjoint equations for internal flow are

$$-(\hat{u}_{j,i} + \hat{u}_{i,j})u_j = -\hat{p}_{,i} + (\nu(\hat{u}_{i,j} + \hat{u}_{j,i}))_{,j} + \hat{c}_{,i}c, \quad (2.45a)$$

$$\hat{u}_{i,i} = 0, \quad (2.45b)$$

$$\hat{c}_{,j}u_j = -(D\hat{c}_{,j})_{,j}. \quad (2.45c)$$

For the inlet we assume a fixed value for the concentration, and the first integral in Eq. (2.44c) becomes zero. To fulfill the second integral, we set the adjoint scalar to zero. This results in the following boundary conditions for the inlet

$$\hat{\mathbf{u}}_t = \mathbf{0}, \quad (2.46a)$$

$$n_i \hat{u}_i = -\frac{\partial J_\Gamma}{\partial p}, \quad (2.46b)$$

$$n_i \hat{p}_{,i} = 0, \quad (2.46c)$$

$$\hat{c} = 0. \quad (2.46d)$$

For the walls, if we assume zero gradient for the scalar transport $n_j \delta c_{,j} = 0$, we need to fulfill the first integral of Eq. (2.44c)

$$\hat{\mathbf{u}}_t = \mathbf{0}, \quad (2.47a)$$

$$n_i \hat{u}_i = -\frac{\partial J_\Gamma}{\partial p}, \quad (2.47b)$$

$$n_i \hat{p}_{,i} = 0, \quad (2.47c)$$

$$0 = \frac{\partial J_\Gamma}{\partial c} + Dn_j \hat{c}_{,j}. \quad (2.47d)$$

Assuming zero concentration, $c = 0$, at the walls would instead lead to $\hat{c} = 0$, to fulfill the second integral in Eq. (2.44c). For the outlet we get,

$$\hat{p} = \frac{\partial J_\Gamma}{\partial(u_i n_i)} + \hat{u}_j u_j + \hat{u}_i n_i u_j n_j + \nu(n_i \hat{u}_i)_{,j} n_j + \hat{c}c, \quad (2.48a)$$

$$0 = \frac{\partial J_\Gamma}{\partial \mathbf{u}_t} + \hat{\mathbf{u}}_t u_j n_j + \nu \hat{\mathbf{u}}_{t,j} n_j, \quad (2.48b)$$

$$0 = \frac{\partial J_\Gamma}{\partial c} + \hat{c}u_j n_j + Dn_j \hat{c}_{,j}. \quad (2.48c)$$

By using the standard OpenFOAM notation, the scalar transport equation can be implemented as

```
tmp<fvScalarMatrix> cEqn
(
    fvm::div(phi, c)
    - fvm::laplacian(Dc, c)
);
cEqn().relax();
solve(cEqn);
```

After implementing the scalar transport, the additional source term is added to the adjoint momentum equations and the adjoint scalar equations implemented as

```
tmp<fvScalarMatrix> caEqn
(
    fvm::div(-phi, ca)
    - fvm::laplacian(Dc, ca)
);
caEqn().relax();
solve(caEqn);
```

The adjoint equations with the boundary conditions presented here and the cost function for scalar uniformity shown in Section 2.4.2 have been implemented in OpenFOAM and are applied in paper IV.

2.3 Application with weakly compressible flows

The derivations presented in previous sections have all assumed incompressible state equations. This section describes the derivation of the adjoint Navier-Stokes equations including scalar transport presented in [19], assuming weakly compressible flow. This implementation is of interest in automotive flow, e.g. to simulate the distribution of NO_x in the exhaust of diesel trucks. This approach is applied to catalyst inlet cones in [19] and intake ports in [53]. In the derivation we assume frozen density, meaning that the variation of the augmented cost function with respect to the density can be neglected. This assumption allows us to leave out the energy equation in the derivation. The momentum, continuity and passive scalar equations are

$$\begin{aligned} \rho u_j \frac{\partial u_i}{\partial x_j} &= -\frac{\partial p}{\partial x_i} + \frac{\partial}{\partial x_j} \left(\mu \left(\frac{\partial u_i}{\partial x_j} + \frac{\partial u_j}{\partial x_i} \right) \right), \\ \frac{\partial(\rho u_j)}{\partial x_j} &= 0, \\ \rho u_j \frac{\partial c}{\partial x_j} &= \frac{\partial}{\partial x_j} \left(D \frac{\partial c}{\partial x_j} \right). \end{aligned} \tag{2.49}$$

The augmented cost function, L , consists of the goal function and the constraints in residual form, Eq. (2.49),

$$L = J + \int_{\Omega} d\Omega \begin{bmatrix} \hat{u}_i \\ \hat{p} \\ \hat{c} \end{bmatrix} \cdot \begin{bmatrix} \rho u_j \frac{\partial u_i}{\partial x_j} + \frac{\partial p}{\partial x_i} - \frac{\partial}{\partial x_j} \left(\mu \left(\frac{\partial u_i}{\partial x_j} + \frac{\partial u_j}{\partial x_i} \right) \right) \\ - \frac{\partial(\rho u_j)}{\partial x_j} \\ \rho u_j \frac{\partial c}{\partial x_j} - \frac{\partial}{\partial x_j} \left(D \frac{\partial c}{\partial x_j} \right) \end{bmatrix} \tag{2.50}$$

The adjoint equations are derived by setting the total variation of the augmented cost function with respect to the flow variables to zero and integrating by parts. The derivation is similar to the one presented in Sections 2.2, 2.2.1 and 2.2.2 and is shown in Appendix A.2. The adjoint equations are

$$-\rho \left(\frac{\partial \hat{u}_j}{\partial x_i} + \frac{\partial \hat{u}_i}{\partial x_j} \right) u_j = -\frac{\partial \hat{p}}{\partial x_i} + \frac{\partial}{\partial x_j} \left(\mu \left(\frac{\partial \hat{u}_i}{\partial x_j} + \frac{\partial \hat{u}_j}{\partial x_i} \right) \right) + \rho c \frac{\partial \hat{c}}{\partial x_j}, \quad (2.51a)$$

$$\frac{\partial \hat{u}_j}{\partial x_j} = 0, \quad (2.51b)$$

$$-\rho u_j \frac{\partial \hat{c}}{\partial x_j} = \frac{\partial}{\partial x_j} \left(D \frac{\partial \hat{c}}{\partial x_j} \right). \quad (2.51c)$$

For the inlet we assume a fixed value for the concentration. This results in the following boundary conditions for the inlet

$$\hat{\mathbf{u}}_t = \mathbf{0}, \quad (2.52a)$$

$$n_i \hat{u}_i = -\frac{\partial J_\Gamma}{\partial p}, \quad (2.52b)$$

$$n_i \hat{p}_{,i} = 0 \quad (2.52c)$$

$$\hat{c} = 0. \quad (2.52d)$$

For the walls, assuming zero gradient for the scalar transport $n_j \delta c_{,j} = 0$, we get

$$\hat{\mathbf{u}}_t = \mathbf{0}, \quad (2.53a)$$

$$n_i \hat{u}_i = -\frac{\partial J_\Gamma}{\partial p}, \quad (2.53b)$$

$$n_i \hat{p}_{,i} = 0 \quad (2.53c)$$

$$0 = \frac{\partial J_\Gamma}{\partial c} + D n_j \hat{c}_{,j}. \quad (2.53d)$$

Assuming zero concentration, i.e. $c = 0$, at the walls would instead lead to $\hat{c} = 0$. For the outlet we get

$$\hat{p} = \frac{\partial J_\Gamma}{\partial (u_i n_i)} + \rho \hat{u}_j u_j + \rho \hat{u}_i n_i u_j n_j + \mu (n_i \hat{u}_i)_{,j} n_j + \rho \hat{c} n_j, \quad (2.54a)$$

$$0 = \frac{\partial J_\Gamma}{\partial \mathbf{u}_t} + \rho \hat{\mathbf{u}}_t u_j n_j + \mu \hat{\mathbf{u}}_{t,j} n_j, \quad (2.54b)$$

$$0 = \frac{\partial J_\Gamma}{\partial c} + \rho \hat{c} u_j n_j + D n_j \hat{c}_{,j}. \quad (2.54c)$$

This implementation is used in paper 5 using the cost function for scalar uniformity at a surface patch, see Section 2.4.3. By leaving out the last term in Eq. (2.51a) and neglecting the boundary conditions for the adjoint scalar, the adjoint Navier-Stokes equations applied in [53] are obtained.

2.4 Cost functions

This section presents the three cost functions that have been implemented in the current work. The adjoint equations including scalar transport, from Section 2.2.2, are

$$\begin{aligned}
 -(\hat{u}_{j,i} + \hat{u}_{i,j})u_j &= -\hat{p}_{,i} + (\nu(\hat{u}_{i,j} + \hat{u}_{j,i}))_{,j} + \hat{c}_{,i}c, \\
 \hat{u}_{i,i} &= 0, \\
 \hat{c}_{,j}u_j &= -(D\hat{c}_{,j})_{,j}.
 \end{aligned} \tag{2.55}$$

The boundary conditions that are applied at the inlet are

$$\begin{aligned}
 \hat{\mathbf{u}}_t &= \mathbf{0}, \\
 n_i \hat{u}_i &= -\frac{\partial J_\Gamma}{\partial p}, \\
 n_i \hat{p}_{,i} &= 0, \\
 \hat{c} &= 0.
 \end{aligned} \tag{2.56}$$

At the walls, the boundary conditions are

$$\begin{aligned}
 \hat{\mathbf{u}}_t &= \mathbf{0}, \\
 n_i \hat{u}_i &= -\frac{\partial J_\Gamma}{\partial p}, \\
 n_i \hat{p}_{,i} &= 0, \\
 0 &= \frac{\partial J_\Gamma}{\partial c} + Dn_j \hat{c}_{,j}.
 \end{aligned} \tag{2.57}$$

For the outlet we get

$$\begin{aligned}
 \hat{p} &= \frac{\partial J_\Gamma}{\partial (u_i n_i)} + \hat{u}_j u_j + \hat{u}_i n_i u_j n_j + \nu(n_i \hat{u}_i)_{,j} n_j + \hat{c}c, \\
 0 &= \frac{\partial J_\Gamma}{\partial \mathbf{u}_t} + \hat{\mathbf{u}}_t u_j n_j + \nu \hat{\mathbf{u}}_{t,j} n_j, \\
 0 &= \frac{\partial J_\Gamma}{\partial c} + \hat{c}u_j n_j + Dn_j \hat{c}_{,j}.
 \end{aligned} \tag{2.58}$$

As noted in the previous sections, the cost functions applied to ducts are often only evaluated at the boundaries, and the contribution from the cost function therefore enters the adjoint equations only through the boundary conditions. The derivatives of the cost functions needed in the boundary conditions are evaluated in the following pages. The boundary conditions for minimization of total pressure drop are applied in papers I-III, the species uniformity at the outlet is applied in paper IV and the species concentration at a surface selection is applied in paper V.

2.4.1 Total pressure drop

An important property of internal flow geometries is the total pressure drop through the geometry. The total pressure drop is measured from the inlet to the outlet, and the cost function can be written as

$$J = \int_{Inlet} c(p/\rho + \frac{1}{2}v^2) d\Gamma - \int_{Outlet} c(p/\rho + \frac{1}{2}v^2) d\Gamma. \quad (2.59)$$

where a constant, $c = 1 \text{ s/m}$, is added to compensate for missing units. The derivative of the cost function for total pressure drop in the boundary conditions at the inlet and walls is

$$\frac{\partial J_\Gamma}{\partial p} = 1 \text{ m/s},$$

and the outlet

$$\frac{\partial J_\Gamma}{\partial(u_i n_i)} = -c u_i n_i, \quad \frac{\partial J_\Gamma}{\partial \mathbf{u}_t} = -c \mathbf{u}_t.$$

This results in the following boundary conditions at the inlet and walls

$$\begin{aligned} \hat{\mathbf{u}}_t &= 0, \\ n_i \hat{u}_i &= -1 \text{ m/s}, \\ n_i \frac{\partial \hat{p}}{\partial x_i} &= 0. \end{aligned} \quad (2.60)$$

At the outlet, we get

$$\begin{aligned} \hat{p} &= -c u_i n_i + \hat{u}_j u_j + \hat{u}_i n_i u_j n_j + \nu \frac{\partial n_i \hat{u}_i}{\partial x_j} n_j, \\ \mathbf{0} &= -c \mathbf{u}_t + \hat{\mathbf{u}}_t u_i n_i + \nu \frac{\partial \hat{\mathbf{u}}_t}{\partial x_j} n_j, \\ n_j \frac{\partial \hat{u}_i n_i}{\partial x_j} &= -\frac{\partial \hat{u}_t}{\partial n_{t_i}}. \end{aligned} \quad (2.61)$$

2.4.2 Species uniformity at the outlet

Species uniformity at the outlet can be described using the following cost function

$$J = \int_{outlet} \frac{1}{2} \left(c - \frac{A_{inlet}}{A_{outlet}} c_{inlet} \right)^2 \quad (2.62)$$

where A is the area of the inlet/outlet and c_{inlet} is the average species concentration at the inlet. The boundary conditions that are applied at the inlet become

$$\begin{aligned} \hat{u}_i &= 0, \\ n_i \hat{p}_{,i} &= 0, \\ \hat{c} &= 0. \end{aligned} \quad (2.63)$$

At the walls, the boundary conditions are

$$\begin{aligned}\hat{u}_i &= 0, \\ n_i \hat{p}_{,i} &= 0, \\ n_j \hat{c}_{,j} &= 0.\end{aligned}\tag{2.64}$$

For the outlet, we get

$$\begin{aligned}\hat{p} &= \hat{u}_j u_j + \hat{u}_i n_i u_j n_j + \nu (n_i \hat{u}_i)_{,j} n_j + \hat{c} c, \\ 0 &= \hat{\mathbf{u}}_t u_j n_j + \nu \hat{\mathbf{u}}_{t,j} n_j, \\ 0 &= c - \frac{A_{\text{inlet}}}{A_{\text{outlet}}} c_{\text{inlet}} + \hat{c} u_j n_j + D n_j \hat{c}_{,j}.\end{aligned}\tag{2.65}$$

2.4.3 Species concentration at a surface selection

A cost function describing the species concentration at the surface can be written as

$$J = \int_{\text{selection}} \frac{1}{2} (c - \bar{c})^2 \tag{2.66}$$

where \bar{c} is the optimal species concentration at the surface. The boundary conditions that are applied at the inlet are

$$\begin{aligned}\hat{u}_i &= 0, \\ n_i \hat{p}_{,i} &= 0, \\ \hat{c} &= 0.\end{aligned}\tag{2.67}$$

At the walls, where the aim is to improve the species distribution, the boundary conditions are

$$\begin{aligned}\hat{u}_i &= 0, \\ n_i \hat{p}_{,i} &= 0, \\ n_j \frac{\partial \hat{c}}{\partial x_j} &= -\frac{1}{D} (c - \bar{c}).\end{aligned}\tag{2.68}$$

At other location of the wall the boundary conditions are the same for \hat{u} and \hat{p} , while the boundary condition for \hat{c} is zero gradient. For the outlet, we get

$$\begin{aligned}\hat{p} &= \hat{u}_j u_j + \hat{u}_i n_i u_j n_j + \nu (n_i \hat{u}_i)_{,j} n_j + \hat{c} c, \\ 0 &= \hat{\mathbf{u}}_t u_j n_j + \nu \hat{\mathbf{u}}_{t,j} n_j, \\ 0 &= \hat{c} u_j n_j + D n_j \hat{c}_{,j}.\end{aligned}\tag{2.69}$$

The adjoint Navier-Stokes equations have now been presented with the boundary conditions applicable for these three cost functions. The last step is now to calculate the gradient of the Lagrangian with respect to the design variables using the results from the primal and the adjoint equations. This is the subject of the following section.

2.5 Sensitivity calculations

The adjoint equations for internal flow have been derived with the appropriate boundary conditions, and the next step is to derive the gradient of the Lagrangian with respect to a design modification. This is equivalent to the step shown in Eq. (2.8). The three approaches that have been used for that purpose in this thesis are briefly introduced in this section. Two of them are derived in the appended papers, while the derivation for the third one is shown in the following section.

2.5.1 Surface sensitivities

To perform shape optimization, it is beneficial to be able to evaluate the gradient of the cost function with respect to the motion of the surface of the geometry. In a design process, this can give information on where to focus with respect to design improvements or when performing fine adjustments on the design. This leads to the surface sensitivities, where the gradient of the cost function with respect to a normal motion of the surface is approximated using only the flow and the adjoint solution on the boundary [39, 50].

The total variation of the Lagrangian can be written as the total variation with respect of the flow variables, \mathbf{w} , and the design parameters, β ,

$$\delta L = \delta_{\mathbf{w}}L + \delta_{\beta}L. \quad (2.70)$$

The variation with respect to the flow variables, \mathbf{w} , was presented in Section 2.2. What is left is the variation with respect to normal displacement of the surface, β ,

$$\delta_{\beta}L = \delta_{\beta}J + \delta_{\beta} \int_{\Omega} (\hat{u}_i, \hat{p}) \mathbf{R} \, d\Omega. \quad (2.71)$$

The total variation of the Navier-Stokes equations, \mathbf{R} , is zero, i.e.

$$\delta \mathbf{R} = \frac{\partial \mathbf{R}}{\partial \mathbf{w}} \delta \mathbf{w} + \frac{\partial \mathbf{R}}{\partial \beta} \delta \beta = 0. \quad (2.72)$$

Rearranging the terms in Eq. (2.72) and inserting into Eq. (2.71) results in

$$\delta_{\beta}L = \delta_{\beta}J - \delta_{\mathbf{w}} \int_{\Omega} (\hat{u}_i, \hat{p}) \mathbf{R} \, d\Omega. \quad (2.73)$$

For ducted flows, the cost function usually has no direct dependence on the normal displacement of the wall. The first term on the right hand side can therefore be left out. If we now include scalar transport, the constraints will consist of the momentum, continuity and scalar transport equations,

$$\begin{aligned} \delta_{\beta}L = & - \int_{\Omega} (\hat{u}_i \delta u_j u_{i,j} + \hat{u}_i u_j \delta u_{i,j} - \hat{u}_i (\nu (\delta u_{i,j} + \delta u_{j,i}))_{,j} \\ & + \hat{u}_i \delta p_{,i} - \hat{p} \delta u_{i,i} + \hat{c} \delta u_j c_{,j} + \hat{c} u_j \delta c_{,j} - \hat{c} (D \delta c_{,j})_{,j}) \, d\Omega. \end{aligned} \quad (2.74)$$

Integrating by parts the terms on the right hand side, as shown in Sections 2.2, 2.2.1 and 2.2.2, the right hand side of Eq. (2.74) can be replaced by the right hand side of Eq. (2.42), excluding the terms including contribution from the cost function. This results in

$$\begin{aligned}
\delta_\beta L = & \int_{\Omega} (\hat{u}_{j,i}u_j + \hat{u}_{i,j}u_j + (\nu(\hat{u}_{i,j} + \hat{u}_{j,i}))_{,j} - \hat{p}_{,i} + \hat{c}_{,i}c)\delta u_i \, d\Omega \\
& - \int_{\Gamma} (n_i\hat{u}_j u_j + \hat{u}_i u_j n_j + \nu(\hat{u}_{i,j} + \hat{u}_{j,i})n_j - \hat{p}n_i + \hat{c}cn_i)\delta u_i \, d\Gamma \\
& + \int_{\Gamma} \nu\hat{u}_i(\delta u_{i,j} + \delta u_{j,i})n_j \, d\Gamma + \int_{\Omega} (\hat{u}_{i,i})\delta p \, d\Omega - \int_{\Gamma} (\hat{u}_i n_i)\delta p \, d\Gamma \quad (2.75) \\
& - \int_{\Omega} (-\hat{c}_{,j}u_j - (D\hat{c}_{,j})_{,j})\delta c \, d\Omega \\
& - \int_{\Gamma} (\hat{c}u_j n_j + Dn_j\hat{c}_{,j})\delta c \, d\Gamma + \int_{\Gamma} \hat{c}Dn_j\delta c_{,j} \, d\Gamma.
\end{aligned}$$

The volume terms in Eq. (2.75) all cancel out as \hat{u} , \hat{p} and \hat{c} fulfill the adjoint equations. This leaves us with only the boundary terms. At the wall, we have that $u_i = 0$ and $\hat{u}_i = 0$, resulting in

$$\begin{aligned}
\delta_\beta L = & - \int_{\Gamma} (\nu(\hat{u}_{i,j} + \hat{u}_{j,i})n_j - \hat{p}n_i) \delta u_i \, d\Gamma \\
& - \int_{\Gamma} Dn_j\hat{c}_{,j}\delta c \, d\Gamma + \int_{\Gamma} \hat{c}Dn_j\delta c_{,j} \, d\Gamma
\end{aligned} \quad (2.76)$$

As proposed in [50] we apply the following Taylor series expansion for the flow variables

$$\begin{aligned}
u_i(0 + \delta\beta) = & u_i(0) + \delta\beta n_j u_{i,j} + \mathcal{O}(\delta\beta^2) \\
\approx & u_i + \delta u_i.
\end{aligned} \quad (2.77)$$

With the variation of the surface, $\delta\beta$, defined in the normal direction of the surface, with a positive direction out of the domain, the variation of the velocity can be written as

$$\delta u_i = \delta\beta n_j u_{i,j}. \quad (2.78)$$

The same approximation is applied for the variation of the passive scalar. If we assume a zero gradient boundary condition for the passive scalar, the second integral vanishes as the same boundary condition is applied for the adjoint scalar resulting in $\hat{c}_{,j} = 0$. For the last term, Eq. (2.78) gives $\delta c = 0$ and we assume the term to be negligible. The contribution from the passive scalar terms can in this case be neglected. If we assume zero concentration at the surface, the last term is zero as $\hat{c} = 0$. Inserting Eq. (2.78) into Eq. (2.76) yields

$$\begin{aligned}
\delta_\beta L = & - \int_{\Gamma} (\nu(\hat{u}_{i,j} + \hat{u}_{j,i})n_j - \hat{p}n_i)\delta\beta n_k u_{i,k} \, d\Gamma \\
& - \int_{\Gamma} Dn_j\hat{c}_{,j}\delta\beta n_k c_{,k} \, d\Gamma.
\end{aligned} \quad (2.79)$$

This expression can be simplified further by following [39]. Applying the decomposition shown in Eqs. (2.26) to (2.28) with $\hat{u}_i = 0$, and the continuity equation $\hat{u}_{i,i} = 0$, results in $n_j(n_i\hat{u}_i)_{,j} = 0$. The first term on the right hand side of Eq. (2.79) can therefore be simplified to $n_j(\hat{\mathbf{u}}_t)_{,j}$ where t denotes the tangential component of \hat{u}_i . The same decomposition is applied to the primal velocity, u_i . By assuming that $\hat{u}_{j,i}n_j = (n_j\hat{u}_j)_{,i}$, the second term can be decomposed into normal and tangential parts as $(n_j\hat{u}_j)_{,i} = n_i(n_j\hat{u}_j)_{,i} + n_t(n_j\hat{u}_j)_{,i}$. Using that $n_i\hat{u}_i = 0$, along the wall, and $n_i(n_j\hat{u}_j)_{,i} = 0$ this term is neglected. The adjoint pressure term becomes zero using the same assumption. The gradient of the cost function with respect to the normal motion of the surface can now be written as

$$\frac{\partial L}{\partial \beta} \approx -\nu n_j \frac{\partial \hat{u}_t}{\partial x_j} n_i \frac{\partial u_t}{\partial x_i} - D n_j \frac{\partial \hat{c}}{\partial x_j} n_i \frac{\partial c}{\partial x_i}. \quad (2.80)$$

For the weakly compressible equations in Section 2.3, we replace the constraints in Eq. (2.73) with Eq. (2.49) and, following the same assumptions as before, this results in

$$\frac{\partial L}{\partial \beta} \approx -\mu n_j \frac{\partial \hat{u}_t}{\partial x_j} n_i \frac{\partial u_t}{\partial x_i} - D n_j \frac{\partial \hat{c}}{\partial x_j} n_i \frac{\partial c}{\partial x_i}. \quad (2.81)$$

2.5.2 Topological sensitivities

Topological optimization can be performed by assigning a momentum loss to cells that have a negative impact on the cost function. This implementation was first presented for finite volume method in [41].

The constraints now include an additional source term representing the porosity,

$$\begin{aligned} u_j \frac{\partial u_i}{\partial x_j} &= -\frac{\partial p}{\partial x_i} + \frac{\partial}{\partial x_j} \left(\nu \left(\frac{\partial u_i}{\partial x_j} + \frac{\partial u_j}{\partial x_i} \right) \right) + \alpha u_i, \\ \frac{\partial u_i}{\partial x_i} &= 0. \end{aligned} \quad (2.82)$$

This additional term results in an additional source term in the adjoint momentum equations,

$$\begin{aligned} -\left(\frac{\partial \hat{u}_j}{\partial x_i} + \frac{\partial \hat{u}_i}{\partial x_j} \right) u_j &= -\frac{\partial \hat{p}}{\partial x_i} + \frac{\partial}{\partial x_j} \left(\nu \left(\frac{\partial \hat{u}_i}{\partial x_j} + \frac{\partial \hat{u}_j}{\partial x_i} \right) \right) + \alpha \hat{u}_i, \\ \frac{\partial \hat{u}_i}{\partial x_i} &= 0. \end{aligned} \quad (2.83)$$

The gradient of the cost function with respect to the porosity in each cell is calculated as

$$\frac{\partial L}{\partial \alpha_i} = -V_i \hat{\mathbf{u}} \cdot \mathbf{u}, \quad (2.84)$$

where V_i is the volume of cell i . This is one of the implementations applied in paper III.

2.5.3 ALE sensitivities

This implementation, which is proposed in paper II, is based on the Arbitrary Lagrangian-Eulerian formulation of the Navier-Stokes equations[5, 6]. In this approach, the constraints are

$$\begin{aligned} (u_j - \alpha_j) \frac{\partial u_i}{\partial x_j} &= -\frac{\partial p}{\partial x_i} + \frac{\partial}{\partial x_j} \left(\nu \left(\frac{\partial u_i}{\partial x_j} + \frac{\partial u_j}{\partial x_i} \right) \right), \\ \frac{\partial u_i}{\partial x_i} &= 0. \end{aligned} \tag{2.85}$$

By assuming that the cell motion is equal to zero the α_j term is neglected in the derivation of the adjoint equations. The gradient of the cost function is calculated with respect to the motion of the cell in a post-processing step as

$$\begin{aligned} \frac{\partial L}{\partial \alpha_i} &= \frac{\partial J}{\partial \alpha_i} + \int_{\Omega} \hat{\mathbf{u}} \cdot \frac{\partial R_{\alpha}}{\partial \alpha_i} d\Omega \\ &= 0 - \int_{\Omega} \hat{\mathbf{u}} \cdot \frac{\partial(\alpha \cdot \nabla \mathbf{u})}{\partial \alpha_i} d\Omega \\ &\approx -\nabla \mathbf{u} \cdot \hat{\mathbf{u}} V_i \end{aligned} \tag{2.86}$$

where V_i is the volume of cell i and the adjoint velocity is obtained from the adjoint equations presented in Section 2.2.

3 Summary of papers

3.1 Paper I

“Aerodynamic Shape Optimization of a Pipe using the Adjoint Method“

Paper A presents results from an optimization of an internal flow geometry using the adjoint method. The surface sensitivities, see Section 2.5.1, are connected to the mesh motion solvers in OpenFOAM[®]. The cost function is total pressure drop and, for that purpose, the appropriate boundary conditions derived in section 2.4.1 are implemented for the adjoint flow field. An inlet pipe to the exhaust gas re-circulator cooler of a truck engine is optimized. The mesh contains 1.0 million hexahedral cells and the inlet velocity is 40 m/s, which is equivalent to boundary conditions at cruising speed, resulting in a Reynolds number of $1.9 \cdot 10^5$. The standard k- ϵ turbulence model [30] was applied and standard wall functions were used for the primal flow field. The total simulation time was 7 hours on 16 cores in which a total of 35 mesh updates were performed. The resulting geometry gives a 6.5% lower total pressure drop compared to the original design.

3.2 Paper II

“Optimization using Arbitrary Lagrangian-Eulerian formulation of the Navier-Stokes equations“

This paper presents a new method to perform shape optimization based on the Arbitrary Lagrangian-Eulerian (ALE) formulation of the Navier-Stokes equations. In the ALE description, the nodes of the computational domain may be moved with the fluid as in the Lagrangian description, held fixed in space as in the Eulerian description or moved in some arbitrary way in between. It is shown that the sensitivities with respect to the mesh motion can be calculated in a post processing step to the primal and adjoint flow simulations. Finally, the sensitivities are coupled to a mesh motion smoothing algorithm, and a duct is optimized with respect to the total pressure drop.

3.3 Paper III

“A comparison of adjoint-based optimizations for industrial pipe flow“

This paper compares the results of three different implementations of adjoint based optimization processes. The aim is to minimize the total pressure drop through an inlet pipe of an exhaust gas recirculation cooler in a diesel engine. In the first implementation, the gradients are evaluated with respect to the motion of the center of the cell using an implementation based on the ALE formulation of

the Navier-Stokes equations. The results are compared to the surface sensitivities, where the gradient of the cost function is evaluated with respect to the normal motion of the surface of the pipe. In the last approach, a topological optimization is performed where the gradient of the cost function is evaluated with respect to a momentum loss in each cell. This gives information that is used when blocking the cells. The results show that the topological optimization was not a feasible choice for this particular case. The methods based on the ALE and the surface sensitivities both obtained a considerable decrease in the total pressure drop. The ALE sensitivities gave a 8.2% decrease, and the surface sensitivities resulted in a 6.5% decrease in the total pressure drop through the pipe.

3.4 Paper IV

“Implementation of an adjoint-based optimization with scalar transport“

This paper presents the results from a validation case for an adjoint scalar transport equation implemented in OpenFOAM[®]. A convection-diffusion equation is used to represent the distribution of particles in a flow and a sensitivity analysis of a particle distribution at the outlet of a two dimensional channel is performed using the adjoint method. The cost function evaluates the non-uniformity of the passive scalar at the outlet. The results are validated by comparing the gradients calculated using the adjoint method to gradients obtained using finite difference calculations. The results show good agreement between the gradients obtained using the two methods.

3.5 Paper V

“Adjoint method for transport of heat and species in internal automotive flows“

Paper V presents results from a sensitivity analysis of a species distribution at the surface of a two dimensional channel. The primal flow is solved using a steady-state compressible flow solver. Adjoint equations applicable to weakly compressible flow have been implemented into OpenFOAM[®]. The implementation includes a cost function describing uniform species distribution at the surface of a geometry. An example of an application for this implementation is to improve NO_X readings in the exhaust of a diesel truck. In the derivation of the adjoint equations, the variation of the density and the turbulent viscosity have been neglected. The gradient of the cost function is calculated with respect to the normal motion of the surface of the channel. The results of the adjoint implementation are validated against gradients approximated using finite difference calculations.

4 Unpublished results

This chapter presents results not included in the appended papers. In Section 4.1, the implementation outlined in paper IV is applied using a Neumann boundary condition at the walls for the scalar, as opposed to a zero concentration at the walls as in paper IV. In Section 4.2, the results from the weakly compressible adjoint solver presented in paper V are compared to results obtained using an incompressible implementation on the same geometry.

4.1 Validation case for scalar transport

In paper IV, a specie distribution was simulated using a two dimensional channel. The gradient of a cost function with respect to the normal motion of the surface was calculated using the adjoint method and the results compared to finite difference calculations. The cost function was uniform distribution of the specie at the outlet. In the case presented in paper IV, the boundary condition for the scalar was set to zero concentration at the wall. In the results presented here, the adjoint implementation was applied to the same case with a zero gradient boundary condition for the specie at the wall boundary. To fulfill the adjoint boundary conditions, this requires the boundary condition for the adjoint scalar to be modified to zero gradient as well. The specie distribution at the inlet is also modified from uniform to being confined only to the lower half of the inlet. A uniform inlet velocity and no-slip boundary condition are applied for velocity. The adjoint equations presented in Section 2.2.2 are applied here. The equations are shown below, along with the boundary conditions from Section 2.4.2.

$$\begin{aligned}
 -\left(\frac{\partial \hat{u}_j}{\partial x_i} + \frac{\partial \hat{u}_i}{\partial x_j}\right) u_j &= -\frac{\partial \hat{p}}{\partial x_i} + \frac{\partial}{\partial x_j} \left(\nu \left(\frac{\partial \hat{u}_i}{\partial x_j} + \frac{\partial \hat{u}_j}{\partial x_i} \right) \right) + c \frac{\partial \hat{c}}{\partial x_j}, \\
 \frac{\partial \hat{u}_j}{\partial x_j} &= 0, \\
 -u_j \frac{\partial \hat{c}}{\partial x_j} &= \frac{\partial}{\partial x_j} \left(D \frac{\partial \hat{c}}{\partial x_j} \right).
 \end{aligned} \tag{4.1}$$

The cost function describes the uniform distribution of species at the outlet,

$$J = \int_{\text{outlet}} \frac{1}{2} (c - 0.5)^2. \tag{4.2}$$

This results in the following boundary conditions for the adjoint equations at the inlet:

$$\begin{aligned}
 u_i &= 0, \\
 n_i \hat{p}_{,i} &= 0, \\
 \hat{c} &= 0.
 \end{aligned} \tag{4.3}$$

At the walls, the boundary conditions are

$$\begin{aligned} u_i &= 0, \\ n_i \hat{p}_{,i} &= 0, \\ n_j \hat{c}_{,j} &= 0. \end{aligned} \tag{4.4}$$

For the outlet, we have

$$\begin{aligned} \hat{p} &= \hat{u}_j u_j + \hat{u}_i n_i u_j n_j + \nu (n_i \hat{u}_i)_{,j} n_j + \hat{c} c, \\ 0 &= \hat{\mathbf{u}}_t u_j n_j + \nu \hat{\mathbf{u}}_{t,j} n_j, \\ 0 &= c - 0.5 + \hat{c} u_j n_j + D n_j \hat{c}_{,j}. \end{aligned} \tag{4.5}$$

The height of the channel at the inlet is $h = 0.05$ m. The inlet velocity is $u = 0.1$ m/s and the Reynolds number is 100 based on the height of the channel. The primal flow field is solved using a steady-state incompressible flow solver. The results from the primal velocity, primal pressure and the primal scalar are shown in Figs. 4.1, 4.2 and 4.3, respectively. The results for the adjoint flow

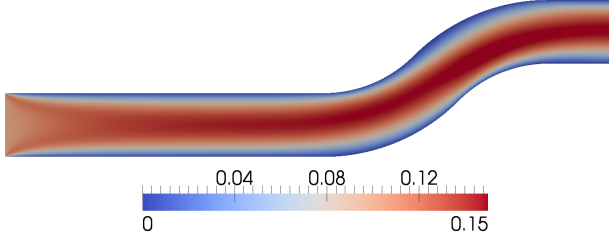


Figure 4.1: *Primal velocity field, u [m/s].*

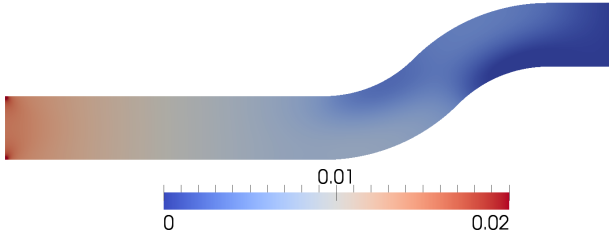


Figure 4.2: *Primal pressure field, p [Pa].*

fields are shown in Figs. 4.4 to 4.6. The surface sensitivities are calculated, using the primal and adjoint velocity fields, from Eq. (2.80) as

$$\frac{\partial L}{\partial \beta} = -\nu n_j \frac{\partial u_i}{\partial x_j} n_m \frac{\partial \hat{u}_i}{\partial x_m}. \tag{4.6}$$

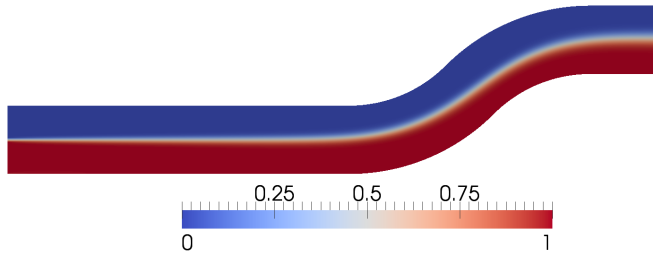


Figure 4.3: *Primal scalar field, c .*

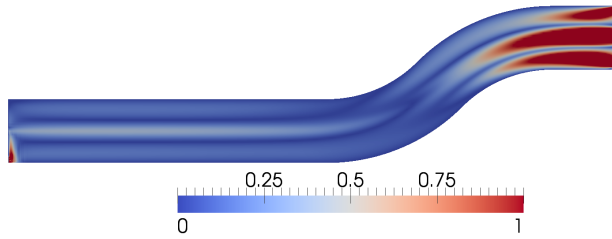


Figure 4.4: *Adjoint velocity field, \hat{u} [m/s].*

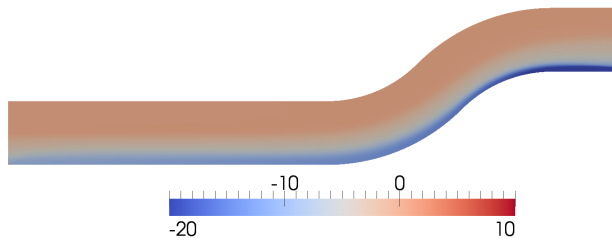


Figure 4.5: *Adjoint pressure field, \hat{p} [Pa].*

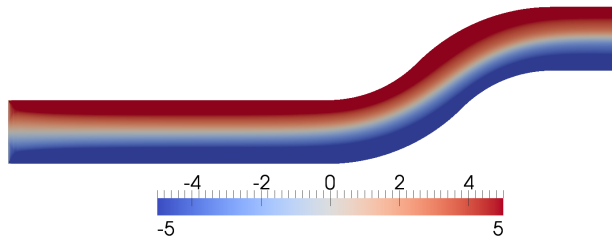


Figure 4.6: *Adjoint scalar field, \hat{c} .*

A first order finite difference approximation is used for comparison, i.e. the gradient of the cost function is approximated as

$$\frac{\partial J}{\partial \beta} \approx \frac{J(\beta + \Delta) - J(\beta)}{\Delta}. \quad (4.7)$$

A step size of $\Delta = 1 \cdot 10^{-7}$ was used. The gradients obtained using the two methods are compared in the region around the bend for the upper and lower surfaces, see Fig. 4.7. The comparison is shown shown in Figs. 4.8 and 4.9. The

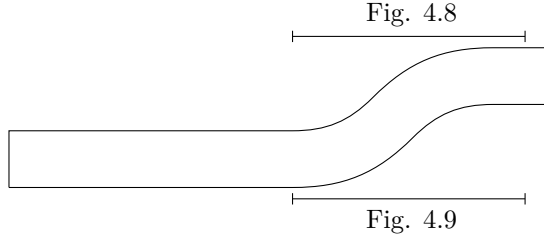


Figure 4.7: *The location at the upper and lower surfaces of the channel where a comparison is made between the surface sensitivities obtained using the adjoint method and the finite difference calculation.*

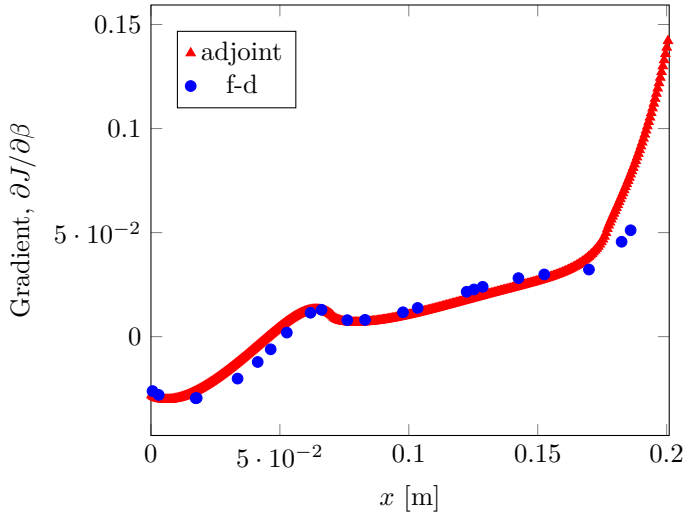


Figure 4.8: *Comparison between sensitivities obtained using the adjoint method and numerical differentiation for the upper part of the domain shown in Fig. 4.7.*

overall accuracy is acceptable and the adjoint method captures the same behavior in the region compared. The results show that the accuracy decreases as we come closer to the outlet and a deviation of roughly 50% can be seen close to the outlet.

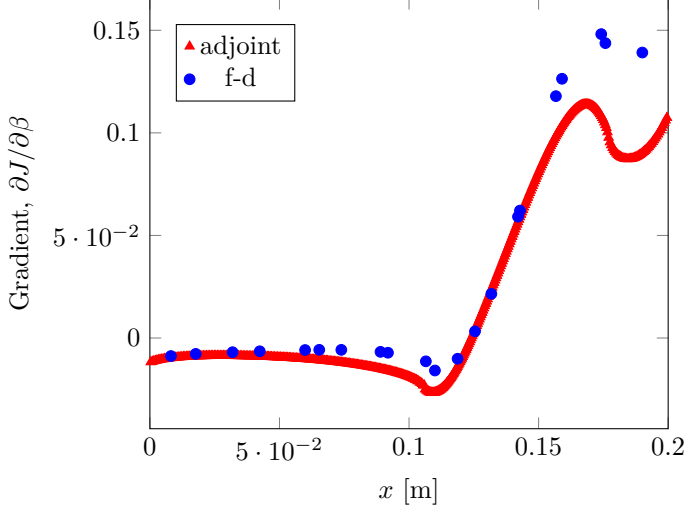


Figure 4.9: Comparison between sensitivities obtained using the adjoint method and numerical differentiation for the lower part of the domain shown in Fig. 4.7.

4.2 Species uniformity at the surface, incompressible solver

Before the weakly compressible adjoint solver was implemented with the cost function presented in Paper V, the cost function was implemented for the incompressible adjoint solver used in the previous papers. The following shows the results from the incompressible solver using the same geometry and boundary conditions as in Paper V. The results are then compared to the results presented in Paper V. The adjoint equations presented in Section 2.2.2 are used along with the boundary conditions from Section 2.4.3. The adjoint equations are

$$\begin{aligned}
 -\left(\frac{\partial \hat{u}_j}{\partial x_i} + \frac{\partial \hat{u}_i}{\partial x_j}\right) u_j &= -\frac{\partial \hat{p}}{\partial x_i} + \frac{\partial}{\partial x_j} \left(\nu \left(\frac{\partial \hat{u}_i}{\partial x_j} + \frac{\partial \hat{u}_j}{\partial x_i} \right) \right) + c \frac{\partial \hat{c}}{\partial x_j}, \\
 \frac{\partial \hat{u}_j}{\partial x_j} &= 0, \\
 -u_j \frac{\partial \hat{c}}{\partial x_j} &= \frac{\partial}{\partial x_j} \left(D \frac{\partial \hat{c}}{\partial x_j} \right).
 \end{aligned} \tag{4.8}$$

The cost function presents the difference between the average concentration at the inlet and the species concentration at a section of the surface,

$$J = \int_{\text{sensor}} \frac{1}{2} (c - 0.5)^2 \, d\Gamma. \tag{4.9}$$

The following boundary conditions are applied at the inlet

$$\begin{aligned}
\hat{\mathbf{u}}_t &= 0, \\
\hat{u}_n &= 0, \\
n_j \frac{\partial \hat{p}}{\partial x_j} &= 0, \\
\hat{c} &= 0.
\end{aligned} \tag{4.10}$$

At the walls, we have

$$\begin{aligned}
\hat{\mathbf{u}}_t &= 0, \\
\hat{u}_n &= 0, \\
n_j \frac{\partial \hat{p}}{\partial x_j} &= 0, \\
n_j \frac{\partial \hat{c}}{\partial x_j} &= 0.
\end{aligned} \tag{4.11}$$

The boundary conditions at the location of the sensor are

$$\begin{aligned}
\hat{\mathbf{u}}_t &= 0, \\
\hat{u}_n &= 0, \\
n_j \frac{\partial \hat{p}}{\partial x_j} &= 0, \\
n_j \frac{\partial \hat{c}}{\partial x_j} &= -\frac{1}{D}(c - 0.5),
\end{aligned} \tag{4.12}$$

and, for the outlet,

$$\begin{aligned}
\hat{p} &= \hat{u}_j u_j + \hat{u}_n u_n + \nu \frac{\partial \hat{u}_n}{\partial x_j} n_j + c \hat{c}, \\
0 &= u_n \hat{\mathbf{u}}_t + \nu \frac{\partial \hat{\mathbf{u}}_t}{\partial x_j} n_j, \\
0 &= u_n \hat{c} + D \frac{\partial \hat{c}}{\partial x_j} n_j.
\end{aligned} \tag{4.13}$$

The geometry consists of a simple two dimensional channel with an inlet at the left and an outlet at the right, see Fig. 4.10. The same mesh is used as in paper V, and the height of the channel is 0.05 m. The velocity is uniform at the inlet, and a no-slip boundary condition is applied at the walls, see Fig. 4.11. This results in a Reynolds number of 85 based on the height of the channel at the inlet. The results for the pressure are shown in Fig. 4.12 and the species concentration in Fig. 4.13. The species concentration is zero at the upper half of the inlet and uniform at the lower half. The adjoint velocity, the adjoint pressure and the adjoint scalar are shown in Figs. 4.14 to 4.16, respectively.

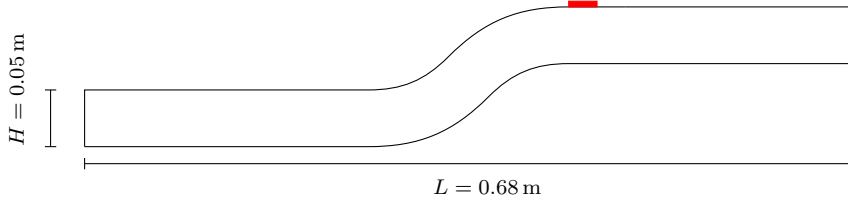


Figure 4.10: *The two-dimensional channel with the inlet at the left and the outlet at the right. The location of the sensor is shown on the upper surface.*

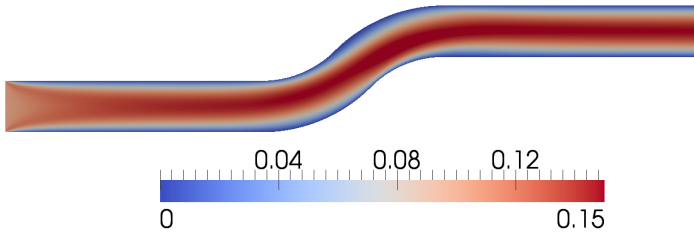


Figure 4.11: *Primal velocity field, u [m/s].*

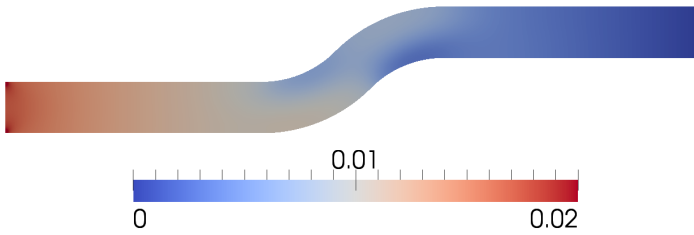


Figure 4.12: *Primal pressure field, p [Pa].*

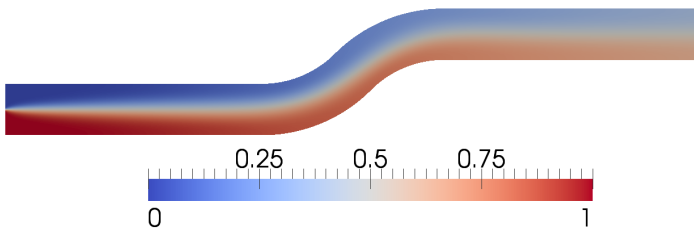


Figure 4.13: *Primal scalar field, c .*

Results from the weakly compressible case are shown in Figs. 4.17 to 4.19 for comparison. The behavior of the adjoint fields is very similar for the incompressible and the compressible case presented in paper V. The adjoint

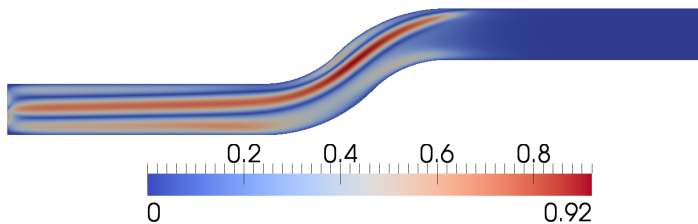


Figure 4.14: *Adjoint velocity field, \hat{u} [m/s].*

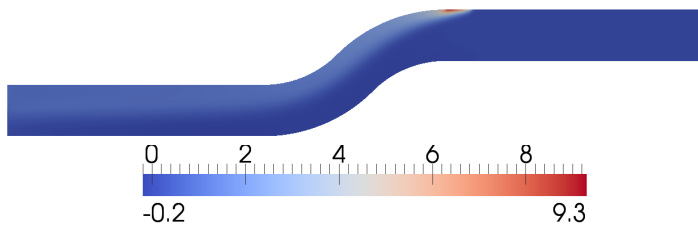


Figure 4.15: *Adjoint pressure field, \hat{p} [Pa].*

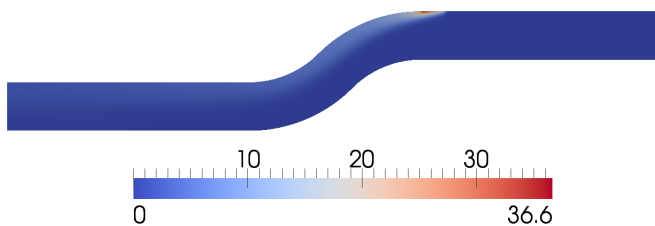


Figure 4.16: *Adjoint scalar field, \hat{c} .*

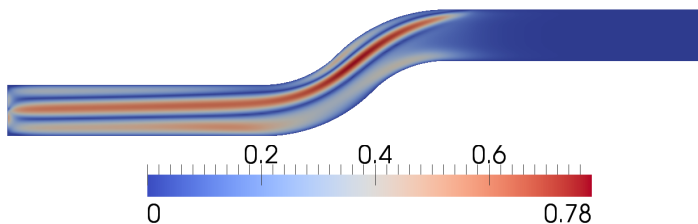


Figure 4.17: *Adjoint velocity field, \hat{u} [m/s], from Paper V.*

velocity and adjoint scalar fields in the case of the compressible case, Figs. 4.17 and 4.19, are roughly a factor ρ lower than in the incompressible case, where $\rho = 1.18\text{kg/m}^3$. On the other hand, the adjoint pressure is roughly the same,

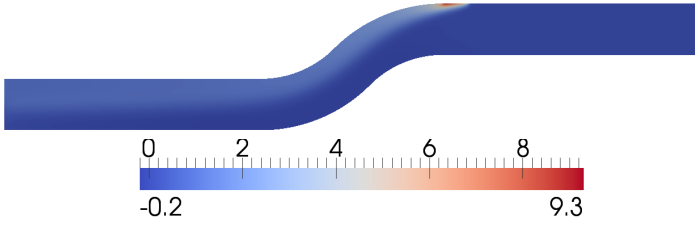


Figure 4.18: Adjoint pressure field, \hat{p} [Pa·kg/m³], from Paper V.

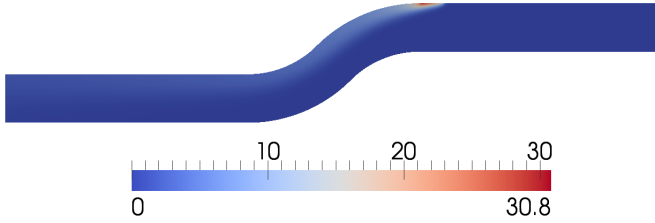


Figure 4.19: Adjoint scalar field, \hat{c} , from Paper V.

which can be explained by the inclusion of the density in the adjoint pressure in the derivation of the weakly compressible adjoint equations. The surface sensitivities are, as in the incompressible cases, calculated from

$$\frac{\partial L}{\partial \beta} = -\nu n_j \frac{\partial u_i}{\partial x_j} n_m \frac{\partial \hat{u}_i}{\partial x_m}. \quad (4.14)$$

Note that ν is replaced by μ in the compressible case. The surface sensitivities from the two cases are compared in the region around the bend, shown in Fig. 4.20. Fig. 4.21 shows the comparison for the upper surface, and the comparison for the lower surface is shown in Fig. 4.22. The comparison shows that the gradient is almost identical, as should be expected for these two cases.

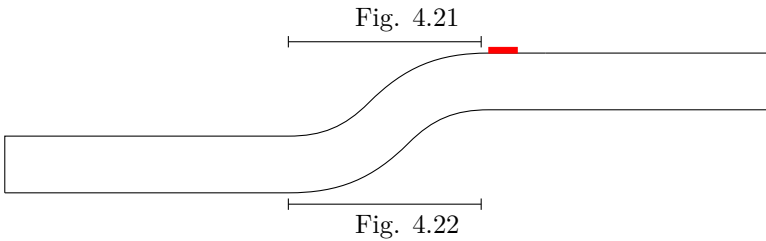


Figure 4.20: The geometry used for the validation. The results from the two adjoint implementations are compared in the region marked by the horizontal lines.

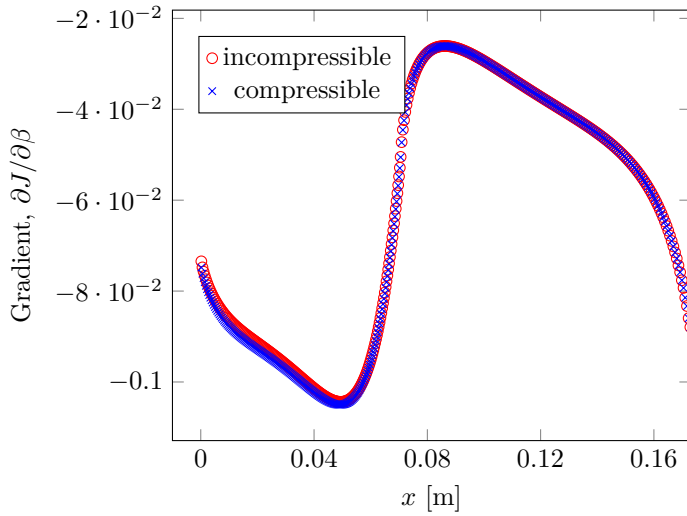


Figure 4.21: Comparison between sensitivities obtained using the incompressible and the weakly compressible implementations for the upper part of the domain shown in Fig. 4.20.

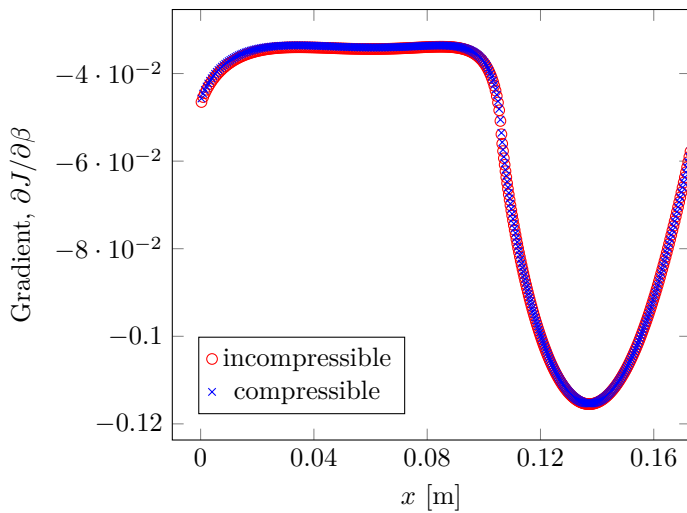


Figure 4.22: Comparison between sensitivities obtained using the incompressible and the weakly compressible implementations for the lower part of the domain shown in Fig. 4.20.

5 Concluding remarks

This thesis focuses on adjoint-based optimization and sensitivity analysis of ducted flows with applications in the automotive industry. The application of the adjoint method allows for cheap calculation of gradients by solving a second set of equations, the so-called adjoint equations. Combining the results from the solution of the adjoint equations and the flow equations makes it possible to calculate the gradient of the cost function with respect to a set of design parameters. Three different implementations have been applied in this work. These implementations are based on normal motion of the surface, momentum loss in each cell and an implementation based on the ALE formulation of the Navier-Stokes equations. The computational cost of this calculation is almost independent of the number of design parameters.

In papers I to III the adjoint method is used to perform gradient calculations in conjunction with an optimization process. The optimization is performed using a steepest descent algorithm. In paper I the adjoint method is applied in the optimization of an inlet pipe to an EGR cooler of a truck. The surface sensitivities are coupled to mesh morphing algorithms in OpenFOAM, and a fine tuning of the geometry is performed. The computational time for the whole optimization process was equivalent to six times the simulation time for the primal flow. In paper II the gradient of the cost function is calculated with respect to the motion of each cell. The cell motion is derived from the Arbitrary Lagrangian-Eulerian formulation of the Navier-Stokes equations. A smoothing algorithm is introduced and the optimization process is applied to a simple pipe. This implementation is compared to the so-called surface sensitivities and the topological optimization based on momentum loss in the cells in Paper III. In this paper the three implementations of the adjoint method are applied to an inlet pipe in a truck. Three optimization processes are performed and the results are compared.

An additional convection-diffusion equation, used e.g. for scalar or species distribution, was added in papers IV and V. In paper IV the relevant adjoint equations were implemented and a cost function based on the scalar distribution at the outlet was evaluated with respect to the normal motion of the surface. The gradients were validated against gradients obtained using a finite difference method for a two dimensional channel. Paper V shows adjoint equations applied for weakly compressible flow, where the primal flow is simulated using a compressible flow solver. A cost function based on uniform species distribution at the surface of the geometry is presented. The gradients of the cost function with respect to normal motion of the surface obtained using the adjoint-based gradients are compared to gradients obtained using a finite difference method. Finally, the unpublished results presented in this thesis show validation cases where the boundary conditions for the scalar transport equation in paper IV have been modified and the flow in paper V simulated using an incompressible flow solver.

References

- [1] Y. Achdou and O. Pironneau. *Computational methods for option pricing*. Vol. 30. Society for Industrial Mathematics, 2005.
- [2] T. Bäck. *Evolutionary algorithms in theory and practice: evolution strategies, evolutionary programming, genetic algorithms*. Oxford University Press on Demand, 1996.
- [3] H. Bensler, T. Eller, A. Kabat vel Job, N. Magoulas, and E. Yigit. “Future perspectives on automotive CAE”. *FISITA World Automotive Congress*. F2014-AST-095. 2014.
- [4] A. Carnarius, B. Gunther, F. Thiele, D. Wachsmuth, F. Tröltzsch, and J. C. de los Reyes. “Numerical Study of the Optimization of Separation Control”. *45th AIAA Aerospace Sciences Meeting and Exhibit*. American Institute of Aeronautics and Astronautics, Jan. 2007. DOI: 10.2514/6.2007-58.
- [5] J. Donea, A. Huerta, J.-Ph. Ponthot, and A. Rodríguez-Ferran. “Arbitrary Lagrangian–Eulerian Methods”. *Encyclopedia of Computational Mechanics*. John Wiley & Sons, Ltd, 2004. ISBN: 9780470091357. DOI: 10.1002/0470091355.ecm009.
- [6] A. Duran. “A numerical formulation to solve the ALE Navier-Stokes equations applied to the withdrawal of magma chambers”. PhD thesis. 2000.
- [7] R. P. Dwight and J. Brezillon. Effect of Various Approximations of the Discrete Adjoint on Gradient-Based Optimization. *AIAA 2006-0690* (2006).
- [8] J. Elliott and J. Peraire. Practical three-dimensional aerodynamic design and optimization using unstructured meshes. *AIAA journal* **35**.9 (1997), 1479–1485.
- [9] K. C. Giannakoglou and D. I. Papadimitriou. “Adjoint Methods for Shape Optimization”. *Optimization and Computational Fluid Dynamics*. Ed. by D. Thévenin and G. Janiga. Springer Berlin Heidelberg, 2008, pp. 79–108. ISBN: 978-3-540-72152-9. DOI: 10.1007/978-3-540-72153-6_4.
- [10] M. B. Giles and N. A. Pierce. An introduction to the adjoint approach to design. *Flow, Turbulence and Combustion* **65** (2000), 393–415.
- [11] M. D. Gunzburger. *Perspectives in Flow Control and Optimization*. Advances in Design and Control. Society for Industrial and Applied Mathematics, 2003.

- [12] E. Helgason and S. Krajnović. “A comparison of adjoint-based optimizations for industrial pipe flow”. *Proceedings of the ASME 2014 4th Joint US-European Fluids Engineering Division Summer Meeting, FEDSM 2014, Collocated with the ASME 2014 12th International Conference on Nanochannels, Microchannels, and Minichannels*. Vol. 1C. Chicago, United States, Aug. 2014. DOI: 10.1115/FEDSM2014-21542.
- [13] E. Helgason and S. Krajnović. “Adjoint method for transport of heat and species in internal automotive flows”. *Proceedings of the First Thermal and Fluids Engineering Summer Conference*. (Submitted). American Society of Thermal and Fluids Engineers. New York, United States, Aug. 2015.
- [14] E. Helgason and S. Krajnović. Aerodynamic Shape Optimization of a Pipe using the Adjoint Method. *ASME 2012 International Mechanical Engineering Congress & Exposition, 9-15 November (2012)*. DOI: 10.1115/IMECE2012-89396.
- [15] E. Helgason and S. Krajnović. “Implementation of an adjoint-based optimization with scalar transport”. *Proceedings of the ASME 2014 International Mechanical Engineering Congress & Exposition*. IMECE2014. Montreal, Quebec, Canada, Nov. 2014.
- [16] E. Helgason and S. Krajnović. Optimization using Arbitrary Lagrangian-Eulerian formulation of the Navier-Stokes equations. *Journal of Fluids Engineering (Accepted)* (2015).
- [17] C. Hinterberger, R. Kaiser, and M. Olesen. Automatic shape optimisation of exhaust systems. *Auto Tech Review* **2.3** (2013), 40–43. ISSN: 2250-3390. DOI: 10.1365/s40112-013-0257-3.
- [18] C. Hinterberger and M. Olesen. “Automatic Geometry Optimization of Exhaust Systems Based on Sensitivities Computed by a Continuous Adjoint CFD Method in OpenFOAM”. *SAE Technical Paper*. SAE International, Apr. 2010. DOI: 10.4271/2010-01-1278.
- [19] C. Hinterberger and M. Olesen. Industrial application of continuous adjoint flow solvers for the optimization of automotive exhaust systems. *CFD & OPTIMIZATION, An ECCOMAS Thematic Conference* **069** (May 2011).
- [20] W. Hucho and G. Sovran. Aerodynamics of Road Vehicles. *Annual Review of Fluid Mechanics* **25.1** (1993), 485–537. DOI: 10.1146/annurev.fl.25.010193.002413.
- [21] ECOpoint Inc. *Emission Standards: European Union: Heavy-Duty Truck and Bus Engines*. 2015. URL: <http://www.dieselnet.com/standards/eu/hd.php> (visited on 01/15/2015).

- [22] D. Jakubek and C. Wagner. Shape Optimization of Train Head Cars using Adjoint-based Computational Fluid Dynamics. *Proceedings of the First International Conference on Railway Technology: Research, Development and Maintenance* (Apr. 2012).
- [23] A. Jameson. Aerodynamic design via control theory. *Journal of Scientific Computing* **3.3** (1988), 233–260. DOI: 10.1007/BF01061285.
- [24] A. Jameson, N. Pierce, and L. Martinelli. Optimum Aerodynamic Design Using the Navier – Stokes Equations. *Theoretical and Computational Fluid Dynamics* (1998), 213–237.
- [25] A. Jameson, S. Shankaran, L. Martinelli, and B. Haimes. Aerodynamic Shape Optimization of Complete Aircraft Configurations using Unstructured Grids. *42nd AIAA Aerospace Sciences Meeting and Exhibit* (Jan. 2004).
- [26] S. Kim, J. Alonso, and A. Jameson. Design optimization of high-lift configurations using a viscous continuous adjoint method (Jan. 2002).
- [27] S. Kim, J. Alonso, and A. Jameson. Two-dimensional high-lift aerodynamic optimization using the continuous adjoint method. *8th Symposium on Multidisciplinary Analysis and Optimization* (Sept. 2000).
- [28] S. Krajnović, E. Helgason, and H. Hafsteinsson. “Aerodynamic Shape Optimization of High-Speed Trains”. *Proceedings of the First International Conference on Railway Technology: Research, Development and Maintenance, Civil-Comp Press, Paper 162*. Stirlingshire, UK, 2012.
- [29] S. Krajnović, R. Lárusson, E. Helgason, and B. Basara. “PANS of Rudimentary Landing Gear”. *6th AIAA Theoretical Fluid Mechanics Conference*. Honolulu, United States, 27 - 30 June 2011.
- [30] B. E. Launder and B. I. Spalding. The Numerical Computation of Turbulent Flows. *Computer Methods in Applied Mechanics and Engineering* **3** (1974), 269–289.
- [31] A. Lincke and T. Rung. “Adjoint-Based Sensitivity Analysis for Buoyancy-Driven Incompressible Navier-Stokes Equations with Heat Transfer”. *Proceedings of the Eighth International Conference on Engineering Computational Technology*. Ed. by B. H. V. Topping. paper 100. Stirlingshire, United Kingdom: Civil-Comp Press, 2012.
- [32] A. C. Marta and S. Shankaran. On the handling of turbulence equations in RANS adjoint solvers. *Computers & Fluids* **74** (Mar. 2013), 102–113. DOI: 10.1016/j.compfluid.2013.01.012.

- [33] A. McNamara, A. Treuille, Z. Popović, and J. Stam. “Fluid control using the adjoint method”. *ACM Transactions On Graphics (TOG)*. Vol. 23. 3. ACM. 2004, pp. 449–456.
- [34] S. K. Nadarajah. “The Discrete Adjoint Approach to Aerodynamic Shape Optimization”. PhD thesis. Stanford University, Jan. 2003.
- [35] S. K. Nadarajah and C. Tatossian. Multi-objective aerodynamic shape optimization for unsteady viscous flows. *Optimization and Engineering* **11** (1 2010), 67–106. DOI: 10.1007/s11081-008-9036-4.
- [36] S. Nadarajah and A. Jameson. A comparison of the continuous and discrete adjoint approach to automatic aerodynamic optimization. *AIAA paper* **667** (2000), 20.
- [37] E. J. Nielsen and W. K. Anderson. Aerodynamic design optimization on unstructured meshes using the Navier-Stokes equations. *AIAA Journal* **37** (Jan. 1999), 1411–1419. DOI: 10.2514/3.14337.
- [38] *OpenFOAM*[®] *The open source CFD toolbox*. URL: <http://www.openfoam.com>.
- [39] C. Othmer. A continuous adjoint formulation for the computation of topological and surface sensitivities of ducted flows. *International Journal for Numerical Methods in Fluids* **58** (2008), 861–877. DOI: 10.1002/fld.1770.
- [40] C. Othmer. Adjoint methods for car aerodynamics. *Journal of Mathematics in Industry* **4.1** (2014), 6. ISSN: 2190-5983. DOI: 10.1186/2190-5983-4-6.
- [41] C. Othmer and T. Grahs. “Approaches to fluid dynamic optimization in the car development process”. *Proceedings of the EUROGEN conference*. Munich, Germany, 2005.
- [42] C. Othmer, E.M. Papoutsis-Kiachagias, and K. Haliskos. “CFD optimization via sensitivity-based shape morphing”. *Proceedings of the 4th ANSA & μETA International Conference*. Thessaloniki, Greece: BETA CAE Systems S.A., 2011.
- [43] C. Othmer, E. de Villiers, and H.G. Weller. “Implementation of a continuous adjoint for topology optimization of ducted flows”. *18th AIAA Computational Fluid Dynamics Conference*. June. 2007.
- [44] J. E. V. Peter and R. P. Dwight. Numerical sensitivity analysis for aerodynamic optimization: A survey of approaches. *Computers & Fluids* **39.3** (Mar. 2010), 373–391. DOI: 10.1016/j.compfluid.2009.09.013.

- [45] O. Pironneau. On optimum profiles in Stokes flow. *Journal of Fluid Mechanics* **59**.01 (1973), 117–128.
- [46] J. Reuther. Aerodynamic shape optimization for supersonic aircraft. *AIAA Paper* **2838** (2002).
- [47] J. Reuther, J.J. Alonso, M. J. Rimlinger, and A. Jameson. Aerodynamic shape optimization of supersonic aircraft configurations via an adjoint formulation on distributed memory parallel computers. *Computers & fluids* **28**.4 (1999), 675–700.
- [48] J. Reuther, A. Jameson, J. Farmer, L. Martinelli, and D. Saunders. Aerodynamic shape optimization of complex aircraft configurations via an adjoint formulation. *34th Aerospace Sciences Meeting and Exhibit* (Jan. 1996).
- [49] B. Soemarwoto. “The Variational Method for Aerodynamic Optimization Using the Navier-Stokes Equations”. Institute for Computer Applications in Science and Engineering (ICASE), NASA Langley Research Center, 1997.
- [50] O. Soto and R. Lohner. On the computation of flow sensitivities from boundary integrals. *42nd AIAA Aerospace Sciences Meeting and Exhibit* AIAA Paper 2004-0112 (2004).
- [51] D. N. Srinath and S. Mittal. An adjoint method for shape optimization in unsteady viscous flows. *Journal of Computational Physics* **229**.6 (Mar. 2010), 1994–2008. DOI: 10.1016/j.jcp.2009.11.019.
- [52] A. Stück. “Adjoint Navier-Stokes Methods for Hydrodynamic Shape Optimization”. Schriftenreihe Schiffbau, Bericht Nr. 661, ISBN 978-3-89220-661-3. PhD thesis. Institute for Fluid Dynamics and Ship Theory, Nov. 2011.
- [53] E. de Villiers and C. Othmer. “Multi-Objective Adjoint Optimization of Intake Port Geometry”. *SAE Technical Paper*. SAE International, Apr. 2012. DOI: 10.4271/2012-01-0905.
- [54] Q. Wang, P. Moin, and G. Iaccarino. Minimal repetition dynamic checkpointing algorithm for unsteady adjoint calculation. *SIAM Journal on Scientific Computing* **31**.4 (2009), 2549–2567.
- [55] A. S. Zymaris, D. I. Papadimitriou, K. C. Giannakoglou, and C. Othmer. Adjoint wall functions: A new concept for use in aerodynamic shape optimization. *Journal of Computational Physics* **229**.13 (July 2010), 5228–5245. DOI: 10.1016/j.jcp.2010.03.037.
- [56] A. S. Zymaris, D. I. Papadimitriou, K. C. Giannakoglou, and C. Othmer. Continuous adjoint approach to the Spalart–Allmaras turbulence model for

incompressible flows. *Computers & Fluids* **38.8** (Sept. 2009), 1528–1538.
DOI: 10.1016/j.compfluid.2008.12.006.

A Derivation of the adjoint Navier-Stokes equations

This chapter includes parts of the derivation of the adjoint method omitted from Chapter 2. Appendix A.1 shows the integration by parts applied in Section 2.2. Appendix A.2 contains the derivation of the adjoint equations used for weakly compressible flow, shown in Section 2.3.

A.1 Integration by parts

This section contains the integration by parts omitted on Page 12 in Section 2.2. Inserting the linearized constraints, Eq. (2.16) and Eq. (2.17), into Eq. (2.15) yields

$$0 = \delta_v J + \delta_p J + \int_{\Omega} (u_i \rho \delta v_j v_{i,j} + u_i \rho v_j \delta v_{i,j} - u_i (\mu (\delta v_{i,j} + \delta v_{j,i}))_{,j} + u_i \delta p_{,i} - q \delta v_{i,i}) d\Omega. \quad (\text{A.1})$$

Now we proceed to “move” the derivatives from the primal flow variables, δv_i and δp , to the adjoint variables, u_i and q , using integration by parts.

We start from Gauss’s theorem, which states that the sum of all sources minus the sum of all sinks equals the net flow out of a region, i.e.

$$\int_{\Omega} u_{i,i} d\Omega = \int_{\Gamma} u_i n_i d\Gamma, \quad (\text{A.2})$$

where Γ is the closed boundary surface of Ω and n_i is the outward normal unit vector to Γ .

The product rule reads:

$$(f, g)_{,i} = f_{,i} g + f g_{,i}. \quad (\text{A.3})$$

The integration by parts is done by reversing the product rule, $f_{,i} g = (f, g)_{,i} - f g_{,i}$, and applying the Gauss theorem, Eq. (A.2), to each of the terms in the integral in Eq. (A.1).

Assuming incompressibility we obtain the following identities:

$$\begin{aligned} \int_{\Omega} u_i \rho \delta v_j v_{i,j} d\Omega &= \int_{\Gamma} \rho n_j u_i \delta v_j v_i d\Gamma - \int_{\Omega} \rho (u_i \delta v_j)_{,j} v_i d\Omega, \\ &= \int_{\Gamma} \rho n_j u_i \delta v_j v_i d\Gamma - \int_{\Omega} \rho u_{i,j} \delta v_j v_i d\Omega - \int_{\Omega} \rho u_i \delta v_{j,j} v_i d\Omega, \\ &= \int_{\Gamma} \rho n_i u_j v_j \delta v_i d\Gamma - \int_{\Omega} \rho u_{j,i} v_j \delta v_i d\Omega. \end{aligned} \quad (\text{A.4a})$$

$$\begin{aligned}
\int_{\Omega} u_i \rho v_j \delta v_{i,j} \, d\Omega &= \int_{\Gamma} \rho u_i v_j \delta v_i n_j \, d\Gamma - \int_{\Omega} \rho (u_i v_j)_{,j} \delta v_i \, d\Omega, \\
&= \int_{\Gamma} \rho u_i v_j \delta v_i n_j \, d\Gamma - \int_{\Omega} \rho u_{i,j} v_j \delta v_i \, d\Omega - \int_{\Omega} \rho u_i v_{j,j} \delta v_i \, d\Omega, \\
&= \int_{\Gamma} \rho u_i v_j n_j \delta v_i \, d\Gamma - \int_{\Omega} \rho u_{i,j} v_j \delta v_i \, d\Omega. \tag{A.4b}
\end{aligned}$$

$$\begin{aligned}
\int_{\Omega} -u_i (\mu (\delta v_{i,j} + \delta v_{j,i}))_{,j} \, d\Omega &= - \int_{\Gamma} \mu u_i (\delta v_{i,j} + \delta v_{j,i}) n_j \, d\Gamma + \int_{\Omega} \mu (u_{i,j} \delta v_{i,j} + u_{i,j} \delta v_{j,i}), \\
&= - \int_{\Gamma} \mu u_i (\delta v_{i,j} + \delta v_{j,i}) n_j \, d\Gamma + \int_{\Gamma} \mu (u_{i,j} + u_{j,i}) n_j \delta v_i \, d\Gamma \\
&\quad - \int_{\Omega} (\mu (u_{i,j} + u_{j,i}))_{,j} \delta v_i \, d\Omega. \tag{A.4c}
\end{aligned}$$

$$\int_{\Omega} u_i \delta p_{,i} \, d\Omega = \int_{\Gamma} u_i n_i \delta p \, d\Gamma - \int_{\Omega} u_{i,i} \delta p \, d\Omega. \tag{A.4d}$$

$$\int_{\Omega} -q \delta v_{i,i} \, d\Omega = - \int_{\Gamma} q n_i \delta v_i \, d\Gamma + \int_{\Omega} q_{,i} \delta v_i \, d\Omega. \tag{A.4e}$$

The cost function can be decomposed into contributions from the interior, Ω , and the boundary, Γ , i.e.

$$J = \int_{\Gamma} J_{\Gamma} \, d\Gamma + \int_{\Omega} J_{\Omega} \, d\Omega. \tag{A.5}$$

Replacing the terms in Eq. (A.1) with the terms from Eq. (A.4) and the decomposed cost function, Eq. (A.5), results in:

$$\begin{aligned}
0 &= \int_{\Omega} \left(\frac{\partial J_{\Omega}}{\partial u_i} - \rho \hat{u}_{j,i} u_j - \rho \hat{u}_{i,j} u_j - (\mu (\hat{u}_{i,j} + \hat{u}_{j,i}))_{,j} + \hat{p}_{,i} \right) \delta u_i \, d\Omega \\
&\quad + \int_{\Gamma} \left(\frac{\partial J_{\Gamma}}{\partial u_i} + \rho n_i \hat{u}_j u_j + \rho \hat{u}_i u_j n_j + \mu (\hat{u}_{i,j} + \hat{u}_{j,i}) n_j - \hat{p} n_i \right) \delta u_i \, d\Gamma \\
&\quad - \int_{\Gamma} \mu \hat{u}_i (\delta u_{i,j} + \delta u_{j,i}) n_j \, d\Gamma \\
&\quad + \int_{\Omega} \left(\frac{\partial J_{\Omega}}{\partial p} - \hat{u}_{i,i} \right) \delta p \, d\Omega + \int_{\Gamma} \left(\frac{\partial J_{\Gamma}}{\partial p} + \hat{u}_i n_i \right) \delta p \, d\Gamma \tag{A.6}
\end{aligned}$$

Alternative formulations of the second term on the right hand side in Eq. (A.6) have been proposed. This term originates from the first term under the integral sign in Eq. (A.1). Here the term is integrated by parts as done in [39, 55, 19]. In Soto et al. [50], the term is integrated by parts, while they suggest that it can be left out for the adjoint equations to resemble the primal equations. In the third approach, applied e.g in [52, 4, 31], the term is not integrated by parts but is kept as it is.

A.2 Weakly compressible flow

This section presents the derivation of the adjoint Navier-Stokes equations for weakly compressible flow omitted in Section 2.3.

The momentum, continuity and scalar transport equations are

$$\begin{aligned}\rho u_j \frac{\partial u_i}{\partial x_j} &= -\frac{\partial p}{\partial x_i} + \frac{\partial}{\partial x_j} \left(\mu \left(\frac{\partial u_i}{\partial x_j} + \frac{\partial u_j}{\partial x_i} \right) \right), \\ \frac{\partial(\rho u_j)}{\partial x_j} &= 0, \\ \rho u_j \frac{\partial c}{\partial x_j} &= \frac{\partial}{\partial x_j} \left(D \frac{\partial c}{\partial x_j} \right).\end{aligned}\tag{A.7}$$

The augmented cost function is written as

$$L = J + \int_{\Omega} d\Omega \begin{bmatrix} \hat{u}_i \\ \hat{p} \\ \hat{c} \end{bmatrix} \cdot \begin{bmatrix} \rho u_j \frac{\partial u_i}{\partial x_j} + \frac{\partial p}{\partial x_i} - \frac{\partial}{\partial x_j} \left(\mu \left(\frac{\partial u_i}{\partial x_j} + \frac{\partial u_j}{\partial x_i} \right) \right) \\ - \frac{\partial(\rho u_j)}{\partial x_j} \\ \rho u_j \frac{\partial c}{\partial x_j} - \frac{\partial}{\partial x_j} \left(D \frac{\partial c}{\partial x_j} \right) \end{bmatrix}\tag{A.8}$$

Now we calculate the total variation of the augmented cost function with respect to the flow variables, u , p and c . The variation of the constraints with respect to the velocity, $\delta_{\mathbf{u}}\mathbf{R}$, is

$$\begin{aligned}\delta_{\mathbf{u}}(R_1, R_2, R_3)^T &= \rho \delta u_j u_{i,j} + \rho u_j \delta u_{i,j} - (\mu(\delta u_{i,j} + \delta u_{j,i}))_{,j}, \\ \delta_{\mathbf{u}}R_4 &= -(\rho \delta u_i)_{,i}, \\ \delta_{\mathbf{u}}R_5 &= \rho \delta u_j c_{,j}.\end{aligned}\tag{A.9}$$

The variation with respect to the pressure, $\delta_p\mathbf{R}$, is

$$\begin{aligned}\delta_p(R_1, R_2, R_3)^T &= \delta p_{,i}, \\ \delta_p R_4 &= 0, \\ \delta_p R_5 &= 0.\end{aligned}\tag{A.10}$$

The variation with respect to the scalar, $\delta_c\mathbf{R}$, is

$$\begin{aligned}\delta_c(R_1, R_2, R_3)^T &= 0, \\ \delta_c R_4 &= 0, \\ \delta_c R_5 &= \rho u_j \delta c_{,j} - (D \delta c_{,j})_{,j}.\end{aligned}\tag{A.11}$$

The total variation with respect to the flow variables is set to zero, i.e. $0 = \delta_{\mathbf{u}}L + \delta_pL + \delta_cL$. The total variation with respect to the flow variables can now

be written as

$$\begin{aligned}
0 = \delta_{\mathbf{u}}J + \delta_p J + \delta_c J + \int_{\Omega} & (\hat{u}_i \rho \delta u_j u_{i,j} + \hat{u}_i \rho u_j \delta u_{i,j} - \hat{u}_i (\mu (\delta u_{i,j} + \delta u_{j,i}))_{,j} \\
& + \hat{u}_i \delta p_{,i} - \hat{p} (\rho \delta u_i)_{,i} \\
& + \hat{c} \rho \delta u_j c_{,j} + \hat{c} \rho u_j \delta c_{,j} - \hat{c} (D \delta c_{,j})_{,j}) d\Omega.
\end{aligned} \tag{A.12}$$

Now we proceed to “move” the derivatives from the primal flow variables, δu_i , δp and δc , to the adjoint variables, \hat{u}_i , \hat{p} and \hat{c} , using integration by parts. The integration by parts is done by reversing the product rule, $f_{,i} g = (f, g)_{,i} - f g_{,i}$, and applying the Gauss theorem to each of the terms in the integral in Eq. (A.12). We obtain the following identities:

$$\begin{aligned}
\int_{\Omega} \hat{u}_i \rho \delta u_j u_{i,j} d\Omega &= \int_{\Gamma} n_j \hat{u}_i \rho \delta u_j u_i d\Gamma - \int_{\Omega} (\hat{u}_i \rho \delta u_j)_{,j} u_i d\Omega, \\
&= \int_{\Gamma} n_j \hat{u}_i \rho \delta u_j u_i d\Gamma - \int_{\Omega} \hat{u}_{i,j} \rho \delta u_j u_i d\Omega - \int_{\Omega} \hat{u}_i (\rho \delta u_j)_{,j} u_i d\Omega, \\
&= \int_{\Gamma} n_i \rho \hat{u}_j u_j \delta u_i d\Gamma - \int_{\Omega} \rho \hat{u}_{j,i} u_j \delta u_i d\Omega. \tag{A.13a}
\end{aligned}$$

$$\begin{aligned}
\int_{\Omega} \hat{u}_i \rho u_j \delta u_{i,j} d\Omega &= \int_{\Gamma} \rho \hat{u}_i u_j \delta u_i n_j d\Gamma - \int_{\Omega} (\hat{u}_i \rho u_j)_{,j} \delta u_i d\Omega, \\
&= \int_{\Gamma} \rho \hat{u}_i u_j \delta u_i n_j d\Gamma - \int_{\Omega} \hat{u}_{i,j} \rho u_j \delta u_i d\Omega - \int_{\Omega} \hat{u}_i (\rho u_j)_{,j} \delta u_i d\Omega, \\
&= \int_{\Gamma} \rho \hat{u}_i u_j n_j \delta u_i d\Gamma - \int_{\Omega} \hat{u}_{i,j} \rho u_j \delta u_i d\Omega. \tag{A.13b}
\end{aligned}$$

$$\begin{aligned}
\int_{\Omega} -\hat{u}_i (\mu (\delta u_{i,j} + \delta u_{j,i}))_{,j} d\Omega &= - \int_{\Gamma} \mu \hat{u}_i (\delta u_{i,j} + \delta u_{j,i}) n_j d\Gamma + \int_{\Omega} \mu (\hat{u}_{i,j} \delta u_{i,j} + \hat{u}_{i,j} \delta u_{j,i}), \\
&= - \int_{\Gamma} \mu \hat{u}_i (\delta u_{i,j} + \delta u_{j,i}) n_j d\Gamma + \int_{\Gamma} \mu (\hat{u}_{i,j} + \hat{u}_{j,i}) n_j \delta u_i d\Gamma \\
&\quad - \int_{\Omega} (\mu (\hat{u}_{i,j} + \hat{u}_{j,i}))_{,j} \delta u_i d\Omega. \tag{A.13c}
\end{aligned}$$

$$\int_{\Omega} \hat{u}_i \delta p_{,i} d\Omega = \int_{\Gamma} \hat{u}_i n_i \delta p d\Gamma - \int_{\Omega} \hat{u}_{i,i} \delta p d\Omega. \tag{A.13d}$$

$$\int_{\Omega} -\hat{p} (\rho \delta u_i)_{,i} d\Omega = - \int_{\Gamma} \hat{p} n_i \rho \delta u_i d\Gamma + \int_{\Omega} \hat{p}_{,i} \rho \delta u_i d\Omega. \tag{A.13e}$$

$$\begin{aligned}
\int_{\Omega} \hat{c} \rho \delta u_j c_{,j} &= \int_{\Gamma} n_j \hat{c} \rho \delta u_j c d\Gamma - \int_{\Omega} (\hat{c} \rho \delta u_j)_{,j} c d\Omega, \\
&= \int_{\Gamma} n_j \hat{c} \rho \delta u_j c d\Gamma - \int_{\Omega} \hat{c}_{,j} \rho \delta u_j c d\Omega - \int_{\Omega} \hat{c} (\rho \delta u_j)_{,j} c d\Omega, \\
&= \int_{\Gamma} n_i \hat{c} \rho c \delta u_i d\Gamma - \int_{\Omega} \hat{c}_{,i} \rho c \delta u_i d\Omega. \tag{A.13f}
\end{aligned}$$

$$\begin{aligned}
\int_{\Omega} \hat{c} \rho u_j \delta c_{,j} &= \int_{\Gamma} \hat{c} \rho u_j n_j \delta c \, d\Gamma - \int_{\Omega} (\hat{c} \rho u_j)_{,j} \delta c \, d\Omega, \\
&= \int_{\Gamma} \hat{c} \rho u_j n_j \delta c \, d\Gamma - \int_{\Omega} \hat{c}_{,j} \rho u_j \delta c \, d\Omega - \int_{\Omega} \hat{c} (\rho u_j)_{,j} \delta c \, d\Omega, \\
&= \int_{\Gamma} \hat{c} \rho u_j n_j \delta c \, d\Gamma - \int_{\Omega} \hat{c}_{,j} \rho u_j \delta c \, d\Omega. \tag{A.13g}
\end{aligned}$$

$$\begin{aligned}
- \int_{\Omega} \hat{c} (D \delta c_{,j})_{,j} &= - \int_{\Gamma} n_j \hat{c} D \delta c_{,j} \, d\Gamma + \int_{\Omega} \hat{c}_{,j} D \delta c_{,j} \, d\Omega, \\
&= - \int_{\Gamma} n_j \hat{c} D \delta c_{,j} \, d\Gamma + \int_{\Gamma} n_j D \hat{c}_{,j} \delta c \, d\Gamma - \int_{\Omega} (D \hat{c}_{,j})_{,j} \delta c \, d\Omega. \tag{A.13h}
\end{aligned}$$

The cost function is decomposed into contributions from the interior, Ω , and the boundary, Γ , i.e.

$$J = \int_{\Gamma} J_{\Gamma} \, d\Gamma + \int_{\Omega} J_{\Omega} \, d\Omega. \tag{A.14}$$

Replacing the terms in Eq. A.12 with the terms from Eq. A.13 and the decomposed cost function, Eq. A.14, results in:

$$\begin{aligned}
0 &= \int_{\Omega} \left(\frac{\partial J_{\Omega}}{\partial u_i} - \rho \hat{u}_{j,i} u_j - \rho \hat{u}_{i,j} u_j - (\mu(\hat{u}_{i,j} + \hat{u}_{j,i}))_{,j} + \rho \hat{p}_{,i} - \rho c \hat{c}_{,i} \right) \delta u_i \, d\Omega \\
&+ \int_{\Gamma} \left(\frac{\partial J_{\Gamma}}{\partial u_i} + \rho n_i \hat{u}_j u_j + \rho \hat{u}_i u_j n_j + \mu(\hat{u}_{i,j} + \hat{u}_{j,i}) n_j - \rho \hat{p} n_i + \rho c \hat{c} n_i \right) \delta u_i \, d\Gamma \\
&- \int_{\Gamma} \mu \hat{u}_i (\delta u_{i,j} + \delta u_{j,i}) n_j \, d\Gamma \\
&+ \int_{\Omega} \left(\frac{\partial J_{\Omega}}{\partial p} - \hat{u}_{i,i} \right) \delta p \, d\Omega + \int_{\Gamma} \left(\frac{\partial J_{\Gamma}}{\partial p} + \hat{u}_i n_i \right) \delta p \, d\Gamma \\
&+ \int_{\Omega} \left(\frac{\partial J_{\Omega}}{\partial c} - \rho \hat{c}_{,j} u_j - (D \hat{c}_{,j})_{,j} \right) \delta c \, d\Omega \\
&+ \int_{\Gamma} \left(\frac{\partial J_{\Gamma}}{\partial c} + \rho \hat{c} u_j n_j + D n_j \hat{c}_{,j} \right) \delta c \, d\Gamma - \int_{\Gamma} \hat{c} D n_j \delta c_{,j} \, d\Gamma \tag{A.15}
\end{aligned}$$

We focus on applications within ducts and pipes and can therefore make the same assumptions as in Section 2.2.1. We therefore leave out the volume contribution of the cost function, and some of the boundary terms are simplified. Now we also assume that the gradient of the density is negligible compared to the gradient of the adjoint pressure, i.e. $\rho \hat{p}_{,i} \approx (\rho \hat{p})_{,i}$, and rewrite the adjoint pressure to include

the density, $\hat{p} \equiv \rho\hat{p}$. This yields the following adjoint equations,

$$\begin{aligned}
-\rho \left(\frac{\partial \hat{u}_j}{\partial x_i} + \frac{\partial \hat{u}_i}{\partial x_j} \right) u_j &= -\frac{\partial \hat{p}}{\partial x_i} + \frac{\partial}{\partial x_j} \left(\mu \left(\frac{\partial \hat{u}_i}{\partial x_j} + \frac{\partial \hat{u}_j}{\partial x_i} \right) \right) + \rho c \frac{\partial \hat{c}}{\partial x_j}, \\
\frac{\partial \hat{u}_j}{\partial x_j} &= 0, \\
-\rho u_j \frac{\partial \hat{c}}{\partial x_j} &= \frac{\partial}{\partial x_j} \left(D \frac{\partial \hat{c}}{\partial x_j} \right).
\end{aligned} \tag{A.16}$$

Note that a contribution from the primal and the adjoint scalar enters as a source term in the momentum equations. In the derivation of the boundary conditions, we assume a fixed inlet velocity, no-slip at walls and zero gradient at the outlet for the primal velocity. A fixed pressure is used at the outlet and a zero gradient elsewhere. For the primal scalar field, a fixed inlet value was assumed and a zero gradient at the outlet and walls. This results in the following boundary conditions for the inlet

$$\begin{aligned}
\hat{\mathbf{u}}_t &= 0, \\
\hat{u}_n &= -\frac{\partial J_\Gamma}{\partial p}, \\
n_j \frac{\partial \hat{p}}{\partial x_j} &= 0, \\
\hat{c} &= 0.
\end{aligned} \tag{A.17}$$

For the walls, we get

$$\begin{aligned}
\hat{\mathbf{u}}_t &= 0, \\
\hat{u}_n &= -\frac{\partial J_\Gamma}{\partial p}, \\
n_j \frac{\partial \hat{p}}{\partial x_j} &= 0, \\
n_j \frac{\partial \hat{c}}{\partial x_j} &= -\frac{1}{D} \frac{\partial J_\Gamma}{\partial c}.
\end{aligned} \tag{A.18}$$

Assuming zero concentration, i.e. $c = 0$, at the walls would instead lead to $\hat{c} = 0$. For the outlet, we get

$$\begin{aligned}
\hat{p} &= \rho \hat{u}_j u_j + \rho \hat{u}_n u_n + \mu \frac{\partial \hat{u}_n}{\partial x_j} n_j + \rho c \hat{c} + \frac{\partial J_\Gamma}{\partial u_n}, \\
0 &= \rho u_n \hat{\mathbf{u}}_t + \mu \frac{\partial \hat{\mathbf{u}}_t}{\partial x_j} n_j + \frac{\partial J_\Gamma}{\partial \mathbf{u}_t}, \\
0 &= \rho u_n \hat{c} + D \frac{\partial \hat{c}}{\partial x_j} n_j + \frac{\partial J_\Gamma}{\partial c}.
\end{aligned} \tag{A.19}$$